Climate Dynamics
https://doi.org/10.1007/s00382-023-07088-9

ORIGINAL ARTICLE

AMO modulation of interdecadal background of persistent heavy rainfall in summer over the Huaihe River Basin

Jingwen Yu[1,2,3] · Qingquan Li[3,4] · Yihui Ding[3] · Zhiping Wen[1] · Zhiqiang Gong[3] · Xiaoting Sun[3] · Xinyong Shen[4] · Lili Dong[3]

Received: 15 July 2023 / Accepted: 24 December 2023

Abstract

This study used observed rainfall, ERA5 reanalysis, and CMIP6 model datasets to investigate the interdecadal variation and underlying mechanism of persistent heavy rainfall (PHR) over the Huaihe River Basin (HRB) in China during July–August, and to examine the role of the Atlantic Multidecadal Oscillation (AMO) in modulating such rainfall. The results indicate that PHR over the HRB exhibited a marked interdecadal variation. The interdecadal increase in PHR was found attributable primarily to interdecadal enhancement of ascending motion, which might have been due to external forcing by the AMO. The AMO can trigger upper-tropospheric mid–high-latitude Rossby wave trains that can lead to an upper-tropospheric anticyclone and a lower-tropospheric cyclone configuration over the HRB. Increased warm advection and greater transport of water vapor from lower latitudes, caused by enhanced southerlies in the middle–lower troposphere over the HRB, can also lead to enhanced ascending motion over the HRB. Meanwhile, an anomalous cyclone over northeastern China triggered by AMO can transport cold air from higher latitudes to the HRB, boosting convection and promoting the development and duration of PHR. By affecting sea surface temperature in the western North Pacific Ocean, the AMO can also indirectly cause a meridional teleconnection pattern in the lower troposphere, which increases the transport of water vapor to the HRB. Numerical model experiments can reproduce both the interdecadal variations in PHR and the mechanisms of the influence of the AMO on PHR, providing a reliable foundation for understanding and forecasting PHR over the HRB.

Keywords Persistent heavy rainfall · Huaihe River · AMO · Interdecadal variation

1 Introduction

Of the seven major river basins in China, the Huaihe River Basin (HRB) has the greatest average population density. Moreover, it is a key grain production area and manufacturing base in China, and also the center of summer rainfall in East Asia (Qian and Wang 2017). The HRB is in a typical climate-vulnerable zone between the humid subtropical monsoon climate to the south and the warm temperate semi-humid monsoon climate to the north. It is also the basin with the most frequent occurrence of droughts and floods among the seven major river basins in China (Ding et al. 2020a). Owing to global warming and the high sensitivity of the HRB to the effects of climate change, the occurrence of catastrophic events, such as the torrential precipitation and flooding in 2003, 2007, 2013, and 2020, has become more common in recent years, causing considerable economic losses (Qian and Wang 2017; Yuan et al. 2019; Ding et al. 2021). Consequently, investigating the occurrence of

✉ Qingquan Li
liqq@cma.gov.cn

✉ Zhiping Wen
zpwen@fudan.edu.cn

1 Department of Atmospheric and Oceanic Sciences and Institute of Atmospheric Sciences, Fudan University, Shanghai 200438, China

2 Chinese Academy of Meteorological Sciences, Beijing 100081, China

3 China Meteorological Administration Key Laboratory for Climate Prediction Studies, National Climate Centre, Beijing 100081, China

4 Collaborative Innovation Center On Forecast and Evaluation of Meteorological Disasters, Nanjing University of Information Science and Technology, Nanjing 210044, China

Published online: 01 February 2024

severe rainfall over the HRB is crucial for the prevention and mitigation of related disasters in China, and for providing reference for research relating to other climate-vulnerable regions globally.

Previous studies found that summer rainfall in eastern China (including the HRB) has substantial interdecadal variation (Wang 2001; Ding et al. 2009; Zhou and Huang 2009; Huang et al. 2011; Chen et al. 2016). In the previous 70 years, two interdecadal transitions in summer rainfall have occurred in eastern China, i.e., in the 1970s and the 1990s (Wang 2001; Zhu et al. 2011; Li et al. 2012; Si and Ding 2013, 2016). The frequency of occurrence of both extreme droughts and floods in the HRB has increased with the intensity of global warming (Ha et al. 2016; Jin et al. 2022). Extreme events such as persistent heavy rainfall (PHR) can have major socioeconomic impact and affect the livelihoods of many individuals. According to Liao et al. (2022), extreme rainfall in summer over the HRB underwent a substantial negative to positive interdecadal phase transition in the late 1990s, and the forcing of cold air southward by the Baikal anticyclone might have been one of the reasons for this interdecadal phase transition. Furthermore, the position and the intensity of atmospheric circulation systems such as the Western North Pacific Subtropical High (WNPSH), East Asian jets, East Asian summer monsoon, and high-latitude blocking can have substantial impact on the interdecadal variation in summer PHR over East Asia (Liang and Wang 1998; Lu 2004; Ding et al. 2021). Previous studies broadly classified the causes of interdecadal variation in summer PHR over East Asia into two categories: enhanced water vapor transport due to changes in the position and intensity of the WNPSH (Ding and Sun 2001; Zheng et al. 2019; Piao et al. 2021), and enhanced regional ascending motion (Liao et al. 2022). However, quantitative examination of their relative contributions remains lacking, and the mechanism of such interdecadal variation has not been comprehensively investigated. The interdecadal variation in rainfall over East Asia has been studied extensively and found to vary considerably between different basins, with rainfall in the Yangtze River Basin (YRB) and the Yellow River Basin showing inverse phase transitions after the 1990s (Ping et al. 2014). Consequently, to improve forecasting accuracy, rainfall in each basin must be investigated independently and explicitly.

Water vapor for summer rainfall over the HRB is mostly derived from the Indian Ocean, Pacific Ocean, and inland evaporation, with the contribution from the oceans exceeding that from inland evaporation for heavy or extreme precipitation events (Liu et al. 2021a, 2021b). Consequently, the role of the oceans in the interdecadal variation in summer rainfall over eastern China has been extensively investigated, both as an essential external forcing factor for long-term climate change, and as the most important source of water vapor. Zhou and Xia (2012) demonstrated that the pre-winter North Pacific Oscillation enhancement before the mid-1970s resulted in the generation of anomalous cyclonic circulation over the western Pacific Ocean and weakened water vapor transport, such that the North Pacific Oscillation showed significant negative correlation with summer rainfall over the HRB, but this relationship weakened quickly after the mid-1970s. Furthermore, anomalous increase in sea surface temperature (SST) in the tropical western Pacific warm pool changes the location and the intensity of the WNPSH, Intertropical Convergence Zone, and East Asia–Pacific teleconnection, thereby affecting rainfall over the basins of the Yangtze and Huai rivers (Wang et al. 2013; Zhang and Guo 2014). However, the relationship between the East Asia–Pacific teleconnection and summer rainfall over East Asia, on the interdecadal time scale, exhibited temporal deterioration after the late 1980s (Yin et al. 2021), prompting interest in the primary external forcing factors of such interdecadal transition in East Asian rainfall.

The Atlantic Multidecadal Oscillation (AMO) is one of the most prominent signals on the interdecadal time scale with major implications regarding global ocean thermal conditions. It describes the interdecadal variability of North Atlantic SST between 0° and 70°N north of the Atlantic Ocean (Enfield et al. 2001), which is distinguished by a spatially coherent pattern with uniformly SST anomalies over the entire North Atlantic basin. AMO has two significant regimes: 10–30 years and 50–80 years (Lin et al. 2019). Dynamical air–sea coupling over the North Atlantic Ocean is quite complicated and AMO is strongly connected to the North Atlantic Oscillation (NAO) and Atlantic meridional overturning circulation (AMOC). The dynamical coupling between NAO, AMOC and AMO provides decadal-scale predictability to the North Atlantic SST and Northern Hemisphere climate (Li et al. 2013). The spatially coherent variation of North Atlantic SST can be explained by the surface heat flux variations associated with NAO and the AMOC-related ocean dynamics (Sun et al. 2015, 2019). Through those intricate interactions and processes, AMO has a significant impact on climate in the regions surrounding the North Atlantic basin and even extends its effect over East Asia and Indo-Pacific Ocean (Sun et al. 2017a, 2017b; Tong et al. 2023). Si and Ding (2016) proposed that AMO could have played an important role in the late 1990s in regulating the phase transition of the Pacific Decadal Oscillation (PDO). Thus, the AMO could have indirectly excited a Pacific–Japan (PJ)-like teleconnection pattern over East Asia, resulting in interdecadal increase (decrease) in summer rainfall over the region of the Yellow

and Huai river basins (Xuan et al. 2011; Zhu et al. 2015; Qiu and Zhou 2019). Moreover, the PDO could also have affected summer rainfall over the basins of the Yangtze and Huai rivers by influencing the East Asian summer monsoon (Ma 2007; Wei and Zhang 2010; Ding et al. 2020b). Si et al. (2020) demonstrated that the AMO might also cause the formation of the Northeast Asian cold vortex and the Baikal anticyclone, altering Northeast Asian summer rainfall by influencing cold air advection and water vapor transport. Thus, in the 1990s, the AMO might have had major influence on the interdecadal variation in East Asian summer rainfall. However, because few studies have investigated the specific relationship between the oceans and PHR over the HRB, it is unclear whether the AMO has played a major role in the interdecadal variation in PHR over the HRB.

Importantly, despite agreement on the interdecadal transition of summer rainfall over the HRB at the end of the 1990s, the PHR indexes obtained might not fully characterize the variation in such PHR owing to differences in the boundaries of the HRB chosen in different studies, and to the direct selection of June–August as the study period in most related research. Ping et al. (2014) and Lu et al. (2022) both showed that choosing alternative time periods and defining different study areas can result in noticeably varied timings for the derived interdecadal transitions. Earlier studies failed to provide quantitative analysis of the relative contributions of the primary influencing factors of interdecadal variation in PHR over the HRB, and examination of the mechanism via which the dominating factor affected the interdecadal variation remains insufficient. Furthermore, as a key external driving factor of interdecadal variation in precipitation and as the main source of water vapor for severe rainfall, the role of the ocean has not yet been fully elucidated in terms of its effect on PHR over the HRB. Therefore, the objectives of this study were to clarify the evolution characteristics of summer PHR over the HRB in different months and in terms of the interdecadal variation characteristics, and to identify the contribution of each influencing factor and the mechanism of interdecadal variation in summer PHR over the HRB using fine-scale precipitation observations and precise boundary data of the basin. Finally, the modulating impact of the AMO on PHR over the HRB was investigated and validated using numerical models as reference for simulation and prediction.

2 Data and methods

2.1 Data

Daily observations of rainfall in China (1961–2021), obtained from the CN05.1 dataset with $0.25° \times 0.25°$ resolution (Wu and Gao 2013), were used to calculate PHR over the HRB. Other datasets used in this study included SST data (1961–2021) derived from the Hadley Centre Sea Ice and SST (HadISST) dataset with $1° \times 1°$ resolution, provided by the UK Met Office Hadley Centre, and the ERA5 reanalysis dataset (1961–2021) with resolutions of $1° \times 1°$ and $2.5° \times 2.5°$ from the European Centre for Medium-Range Weather Forecasts (Hersbach et al. 2020). The variables extracted from the ERA5 dataset comprised specific humidity, wind, geopotential height, air temperature, surface pressure, and vertical velocity. Furthermore, the results of the hist-resAMO experiments of the medium-resolution climate system model BCC-CSM2-MR, provided by the China Meteorological Administration to the Coupled Model Intercomparison Project Phase 6 (CMIP6) of the World Climate Research Program, were used to validate the results based on the observations and reanalysis dataset. The hist-resAMO experiment is a pacemaker-coupled historical climate simulation but with SSTs restored to model climatology and observational historical anomalies superimposed in the AMO domain. The time period of hist-resAMO extends the regular AMIP experiment (that is, using the observed historical SST to drive the atmospheric model) forward to 1870 (Zhang et al. 2019). The results of hist-resAMO can be compared with the data of observation, so as to understand the source of interdecadal monsoon variation, especially the role of AMO in the interdecadal variation of monsoon (Zhou et al. 2019). Therefore, this study uses the results of hist-resAMO experiments to validate the mechanism of positive and negative phase transition of AMO influencing on PHR over the HRB.

The data used in this study were subjected to 11-year filtering using the Lanczos filter after removal of the linear trend. Summer was defined as June–August.

2.2 Methods

2.2.1 Definition of PHR over the HRB

The HRB boundary data, given by the Institute of Geographic Sciences and Natural Resources Research-Resource and Environmental Science and Data Center of China (https://www.resdc.cn/DataList.aspx), encompass parts of Shandong, Henan, Anhui, and Jiangsu provinces in China. Through consideration of the findings of previous studies (Bao 2007; Chen and Zhai 2013; Ren et al. 2013; Yao and Ren 2019), PHR over the HRB was defined in this study as rainfall of > 15 mm day^{-1} at a specific grid point with duration of at least three days; the interdecadal variation time series of cumulative PHR over the HRB was used as the PHR index.

2.2.2 Moisture budget equation

After decomposing the moisture budget equation to extract the local rainfall variation determinants, the simplified water vapor budget equation in P-coordinates can be expressed as follows (Chou and Lan 2012):

$$P = -\int_{p_b}^{p_t} V \cdot \nabla q - \int_{p_b}^{p_t} W \cdot \frac{\partial q}{\partial p} + E + \delta \tag{1}$$

where $-\int_{p_b}^{p_t} V \cdot \nabla q$ represents the water vapor advection term, $-\int_{p_b}^{p_t} W \cdot \frac{\partial q}{\partial p}$ represents the vertical water vapor transport term, E represents the evaporation term, δ represents the turbulent diffusion term (which can be neglected), P represents precipitation, p_t and p_b represent the top and the bottom of the vertical integration layer (taken as 300 and 1000-hPa), respectively, V represents wind vectors, q is specific humidity, and p is air pressure.

2.2.3 Partial correlation

The higher-order partial correlation was employed in this study, which determines the correlation coefficients between any two variables among several variables after removing the influence of other factors. Generally, supposing there are k ($k > 2$) variables $x_1, x_2, \ldots, x_k$, then when two variables x_i and x_j are considered, the $g-$order($g \leqslant k-2$) partial correlation coefficient can be calculated as follows:

$$r_{ijl_1l_2\ldots l_g} = \frac{r_{ijl_1l_2\ldots l_{g-1}} - r_{il_gl_1l_2\ldots l_{g-1}} r_{jl_gl_1l_2\ldots l_{g-1}}}{\sqrt{\left(1 - r^2_{il_gl_1l_2\ldots l_{g-1}}\right)\left(1 - r^2_{jl_gl_1l_2\ldots l_{g-1}}\right)}} \tag{2}$$

The partial correlation coefficients of order $g-1$ are all found on the right-hand side of Eq. (2).

2.2.4 Effective freedom degrees

After interdecadal filtering, the effective freedom degrees of the data must be recalculated, and the approximation formula can be expressed as follows (Pyper and Peterman 1998):

$$\frac{1}{N^{eff}} \approx \frac{1}{N} + \frac{2}{N}\sum_{j=1}^{N} \frac{N\text{-}j}{N} \rho_{xx}(j)\rho_{yy}(j) \tag{3}$$

where N is the overall sample count, $\rho_{xx}(j)$ and $\rho_{yy}(j)$ represent the autocorrelations of time series x and y, respectively, and j represents the lag time.

Empirical orthogonal function analysis, the sliding t-test, power spectrum analysis, the Lanczos filter, correlation analysis, synthetic analysis, the t-test, and the F-test were also used in this study.

3 Results

3.1 Variation in PHR over the HRB in summer

Figure 1 depicts the spatial distribution of PHR, the total rainfall for each month in summer, and the proportion of PHR to total rainfall in the HRB. The locations of the high-value centers of PHR are broadly similar to those of total rainfall, and the movement of the PHR rainband is consistent with that of total rainfall. The rainband moves steadily northward with time and arrives at the southern edge of the HRB (south of the Huaihe River) in June; it moves to the central HRB in July; and the high-value center appears over the northeastern HRB in August. The PHR center is somewhat southward in comparison with that of the total rainfall in July and is concentrated over the Huaihe River. The PHR and the total rainfall in June account for lesser fractions of the total PHR and the total rainfall over the HRB during summer, i.e., 11.38% and 22.92%, respectively (Table 1). Rainfall over the HRB is mostly concentrated in July and August (77.08%), with the proportion of PHR in July and August accounting for 82.93% of the total summer PHR. The proportion of PHR in the total rainfall during summer is approximately 11.24%, with the proportion of PHR in the total rainfall during July–August reaching 12.09%, indicating that PHR is an extreme event that can have substantial impact on production, life, and the economy in the HRB.

The time series of PHR variation by month in summer over the HRB is shown in Fig. 2. Except for a few extreme years, it is evident that PHR is concentrated in July–August and has no notable long-term trend in all months. The frequency of PHR in June (figure not shown) and the total PHR (Fig. 2a) are lower than those in July–August, when the average rainfall is only one quarter of that in July and one half of that in August. PHR occurs mostly in July over the HRB and is rather consistent (Fig. 2b). Although the long-term trend is close to zero, PHR over the HRB in July declined considerably after 1970, with average values of 42.59 mm in 1961–1970 and 13.88 mm in 1971–1980, i.e., a reduction of 67.41%. Conversely, PHR over the HRB in July increased dramatically after 1999, with average values of 20.76 mm in 1989–1998 and 39.48 mm in 1999–2008. The averaged total PHR in 1999–2008 is twice as large as that in 1989–1998. This demonstrates the considerable interdecadal variation in PHR over the HRB in July, which remains in the cumulative PHR in July–August (Table 2). Therefore, Table 2 compares PHR in 4 periods, in which the periods 1961–1970 and 1971–1980 are used to quantitatively analyze the interdecadal variation of PHR around 1970s, and the other two periods 1989–1998 and 1999–2008 are used to quantitatively analyze the

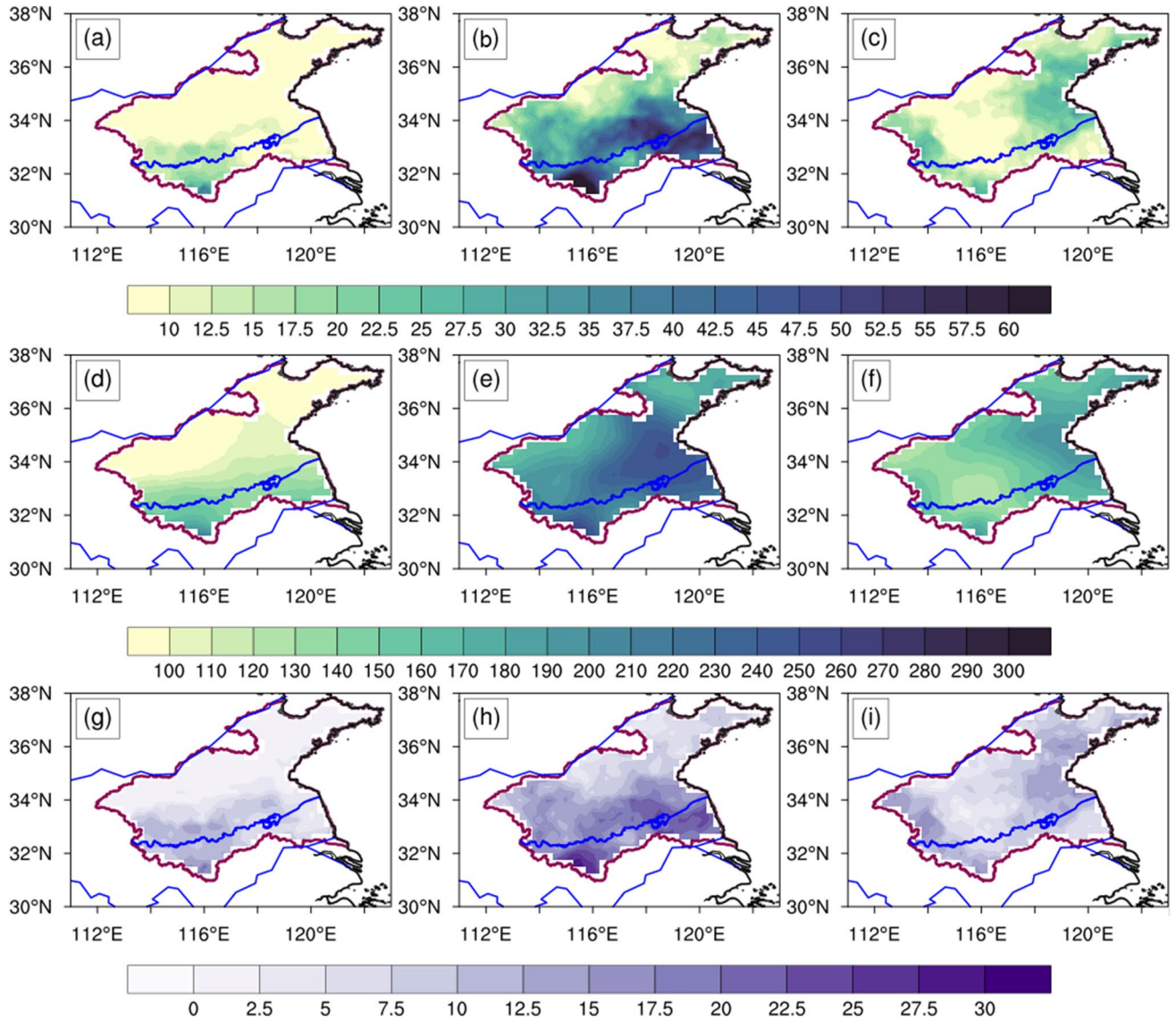

Fig. 1 Spatial distribution of climatological (**a**–**c**) PHR (unit: mm), (**d**–**f**) total rainfall (unit: mm), and (**g**–**i**) proportion of PHR in total rainfall (unit: %) for (**a, d, g**) June, (**b, e, h**) July, and (**c, f, i**) August during 1961–2021 (red and blue lines indicate the boundary of the HRB and the main rivers, respectively)

Table 1 Climatological PHR and total rainfall (unit: mm) averaged over the HRB and their ratios (unit: %) in June, July, and August during 1961–2021

Month	June	July	August	July–August	June–August
Total PHR	6.03	28.28	14.50	43.92	52.96
Total summer rainfall	107.99	206.34	156.82	363.16	471.16
Ratio of PHR to total summer PHR	11.38	53.40	27.38	82.93	–
Ratio of rainfall to total summer rainfall	22.92	43.79	33.28	77.08	–

interdecadal variation of PHR around 2000s. PHR over the HRB in August shows a decreasing trend, which is not statistically significant. Generally, both PHR and total rainfall are low in June. Consequently, PHR in July dominates the interdecadal variation characteristics of summer PHR over the HRB, and PHR in August dominates its long-term trend. However, because the trend is not significant and in one third of the years from 1961 to 2021 PHR events span July and August, the interdecadal variation in PHR in July–August over the HRB is the focus of the following analysis.

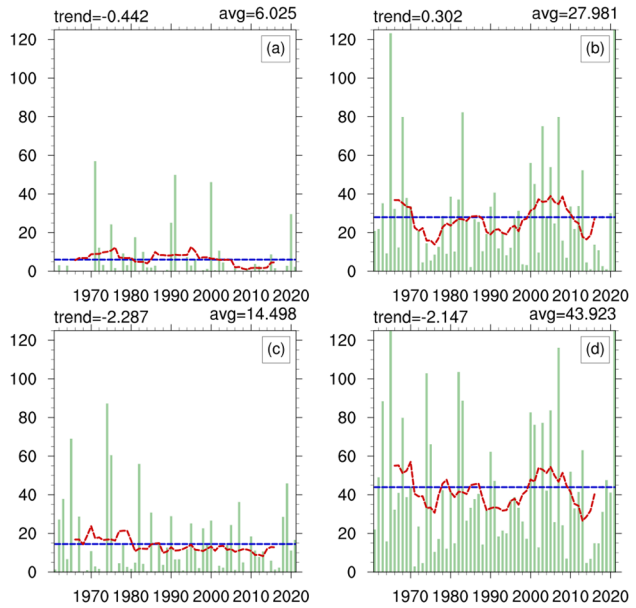

Fig. 2 Time series of regional mean PHR in **a** June, **b** July, **c** August, and **d** July–August during 1961–2021 (blue lines represent multiyear average, unit: mm; red line represents 11-year running average, unit: mm)

Table 2 Average PHR over the HRB in July–August in various periods (unit: mm)

Period	1961–1970	1971–1980	1989–1998	1999–2008
Average PHR	62.07	32.54	33.58	55.73

The time series and power spectrum of regionally averaged July–August PHR over the HRB are shown in Fig. 3a and c, respectively. The power spectrum has the characteristic of periodic variation in PHR with two notable variation cycles of 17–20 and 3–4 years. It demonstrates that PHR over the HRB has significant interdecadal and interannual variability, and that the interannual variation in PHR is generally stronger in the interdecadal positive phase than in the interdecadal negative phase. It suggests that the interdecadal variation, as the climatic background of interannual variation, has a moderating effect on the interannual variation, and thus the study of interdecadal variation is important. Figure 3b depicts the interdecadal variation of regionally averaged July–August PHR after 11–year filtering. PHR over the HRB experienced significant interdecadal transition in 1998/1999 (Fig. 3d), indicating that PHR increased significantly after 1999, and validated with station data. In this study, the PHR index was defined as the normalized time series in Fig. 3b. This study did not focus on the transition around 2010 owing to data length constraints and interdecadal filtering loss.

The spatial distribution of PHR in July–August (Fig. 4a) is more uniform than that in June, July, and August, and the interdecadal variance of PHR in July–August has a maximum weight of 46% of the total variance (Fig. 4b). It indicates that the interdecadal variance of PHR accounts for a substantial proportion of the total rainfall variance, and that the areas of high rainfall are primarily located in the central and southwestern HRB. A higher proportion of variance means that the component accounts for a greater part of the variation in the initial data; hence, the interdecadal variation in PHR over the HRB cannot be ignored.

3.2 Mechanisms of interdecadal variation in PHR over the HRB

Regressions of the upper- and lower-tropospheric circulation and geopotential height against the PHR index in July–August reveal a significant "positive–negative–positive–negative–positive–negative" (denoted as "+–+–+–") wave train propagating from the North Atlantic Ocean to East Asia in the middle and higher latitudes of the Northern Hemisphere, with negative geopotential height centers over the North Atlantic East Coast, Central Asia, and Sea of Okhotsk and positive centers over the western North Atlantic, Northern Europe, and Lake Baikal. The circulation in the middle troposphere (500-hPa, Fig. 5b) is similar to that at 200-hPa, albeit with minor increase in the WNPSH in middle–lower latitudes due to anomalous southeasterly transport from the western Pacific Ocean to the HRB. The HRB is to the southeast of the anomalous anticyclone centered over Lake Baikal, and the northwestern HRB is influenced by anomalous northeasterlies from the southeastern edge of that anomalous anticyclone, while southern and eastern parts of the HRB are controlled by anomalous southeasterlies and southwesterlies, respectively, circulating around the western edge of the WNPSH. The anomalous anticyclone over Lake Baikal and the anomalous cyclone over the Sea of Okhotsk transport cold air from high latitudes, while the anomalous enhancement of the WNPSH transports warm humid air from low-latitude oceans to the HRB, where the cold and warm air masses converge, stimulating convection and producing rainfall. The circulation in the lower troposphere (850-hPa, Fig. 5c) over the East Asian coast, from the low-latitude maritime continent to the northern Sea of Okhotsk, exhibits a PJ-like pattern in the distribution of anomalous geopotential height, with the Yellow Sea, East China Sea, and Northwest Pacific controlled by an anomalous anticyclone. Eastern parts of the HRB are to the west of the anomalous anticyclone and are affected by anomalous southwesterlies, indicating notable enhancement of the southwesterly jet in the lower troposphere and corresponding anomalous enhancement of southwesterly water vapor transport (Fig. 5d). On the one hand, the anomalous blocking in

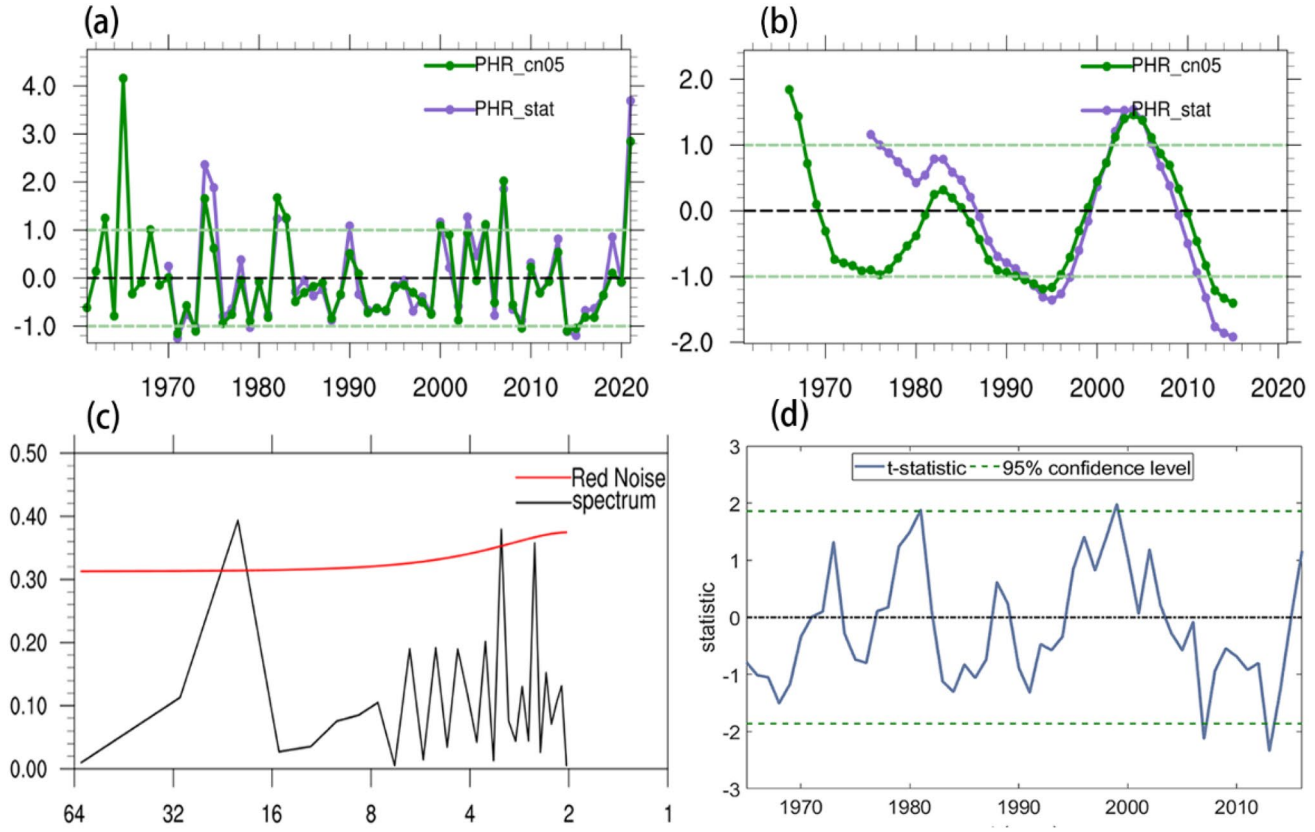

Fig. 3 **a** Time series of regionally averaged PHR over the HRB in July–August during 1961–2021 (un-detrended, unfiltered, and normalized. Purple lines represent the results based on observation station data, while the green lines represent the result based on CN05.1 grid data), **b** the interdecadal component of **a** (detrended, removed 11-year filtering, and normalized), **c** the power spectrum of **a**, and **d** the sliding t-test of **a**

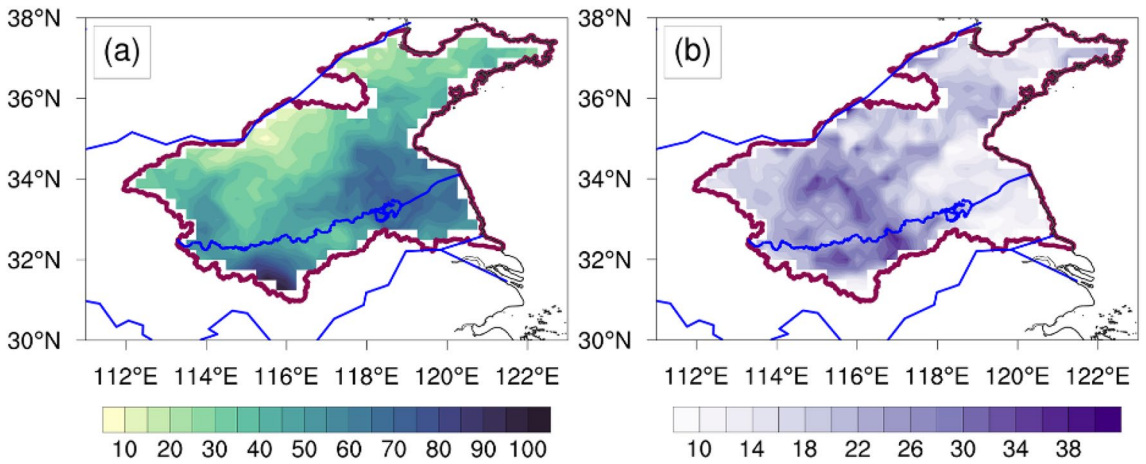

Fig. 4 **a** Spatial distribution of climatological PHR (unit: mm) over the HRB in July–August during 1961–2021, and **b** variance ratio (unit: %) between interdecadal and total PHR

the middle–upper troposphere over Lake Baikal has potential to transport cold air from higher latitudes (Siberia and the Sea of Okhotsk) to the HRB, while the anomalous enhancement of the WNPSH in the middle–lower troposphere can carry warm and humid air from low-latitude oceans to the HRB. Meanwhile, the lower troposphere is controlled by an anomalous cyclone over Central Asia, and the anomalous cyclonic circulation forced by the large topographic

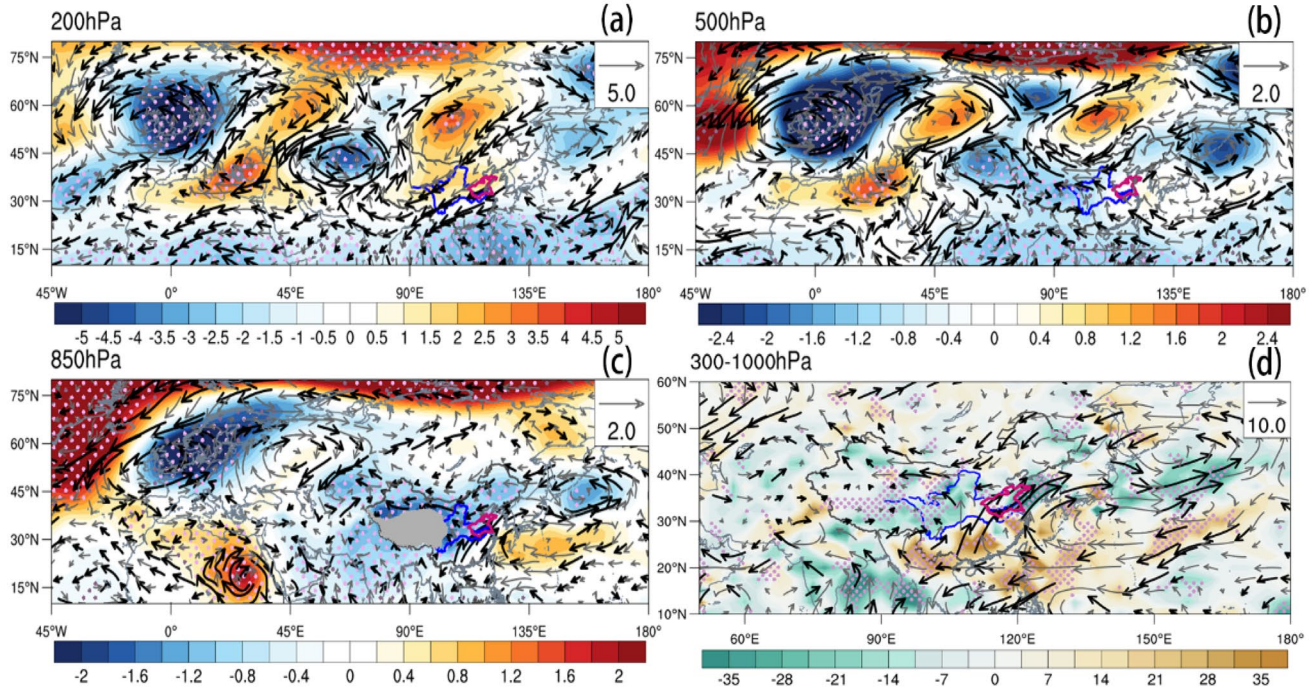

Fig. 5 Regressions of **a** 200-hPa, **b** 500-hPa, **c** 850-hPa wind (vector, unit: m s^{-1}) and geopotential height (shading, unit: gpm), and **d** 300–1000-hPa vertically integrated water vapor flux (vector, unit: kg $m^{-1}s^{-1}$) and its dispersion (shading, unit: kg $m^{-1}s^{-1}$) against the PHR index in July–August of 1979–2020 (dots and bold vectors indicate significance at the 95% confidence level; the dark pink curve indicates the location of the HRB)

effect of the Tibetan Plateau can transport warm humid air from the Bay of Bengal to the HRB, facilitating convection enhancement over the HRB. On the other hand, the upper troposphere over the HRB is governed by an anomalous anticyclone, while the lower troposphere is controlled by an anomalous cyclone. The circulation situation of upper-atmospheric divergence and lower-atmospheric convergence promotes the establishment and maintenance of ascending motion, which also generates a rainfall-friendly atmospheric circulation configuration. The Yellow Sea, East China Sea, Northwest Pacific Ocean, and South China are the primary sources of the water vapor found over the HRB, as evidenced by the water vapor fluxes dispersion field (Fig. 5d). The strong southerly water vapor conveyor belt delivers water vapor from low-latitude oceans to the HRB. The vertical motion and the lower-tropospheric southerlies play crucial roles in the interdecadal variation in PHR over the HRB.

The moisture budget equation is decomposed to diagnose the underlying causes of interdecadal variation in PHR over the HRB (Fig. 6, Table 3), and the results show that PHR over the HRB is primarily influenced by the vertical water vapor transport term on the interdecadal time scale, with its contribution reaching 83.68%. The water vapor advection term and the evaporation term have weak and substantial negative relationships with PHR, respectively. The spatial distribution of the correlation coefficients also shows that PHR over the HRB has a stronger positive correlation with the vertical water vapor transport term than with the water vapor advection term in July–August, while the center of significant positive correlation for the water vapor advection term is over the Yellow Sea. This is consistent with the result of the regression of water vapor fluxes against the PHR index, which indicate that the center of convergence is similarly over the Yellow Sea, showing that the interdecadal amplification in PHR over the HRB in July–August is mostly attributable to abnormal enhancement of ascending motion over the HRB. Furthermore, while PHR over the HRB has significant negative correlation with evaporation within the basin, it has significant positive correlation with evaporation from neighboring rivers or oceans such as the YRB, Northwest Pacific Ocean, and South China Sea (figure not shown), which is consistent with the water vapor fluxes dispersion region shown in Fig. 5d, indicating that these regions are important sources of water vapor for the HRB.

The vital role of the vertical water vapor transport term provides further explanation of the link between vertical velocity and PHR over the HRB (Fig. 7b). Additionally, Kosaka et al. (2011) demonstrated that temperature advection in the mid-troposphere has substantial impact on the position and the magnitude of rainbands over the YRB. Therefore, the influence of thermal effects on vertical motion over the HRB is discussed, but excluding the

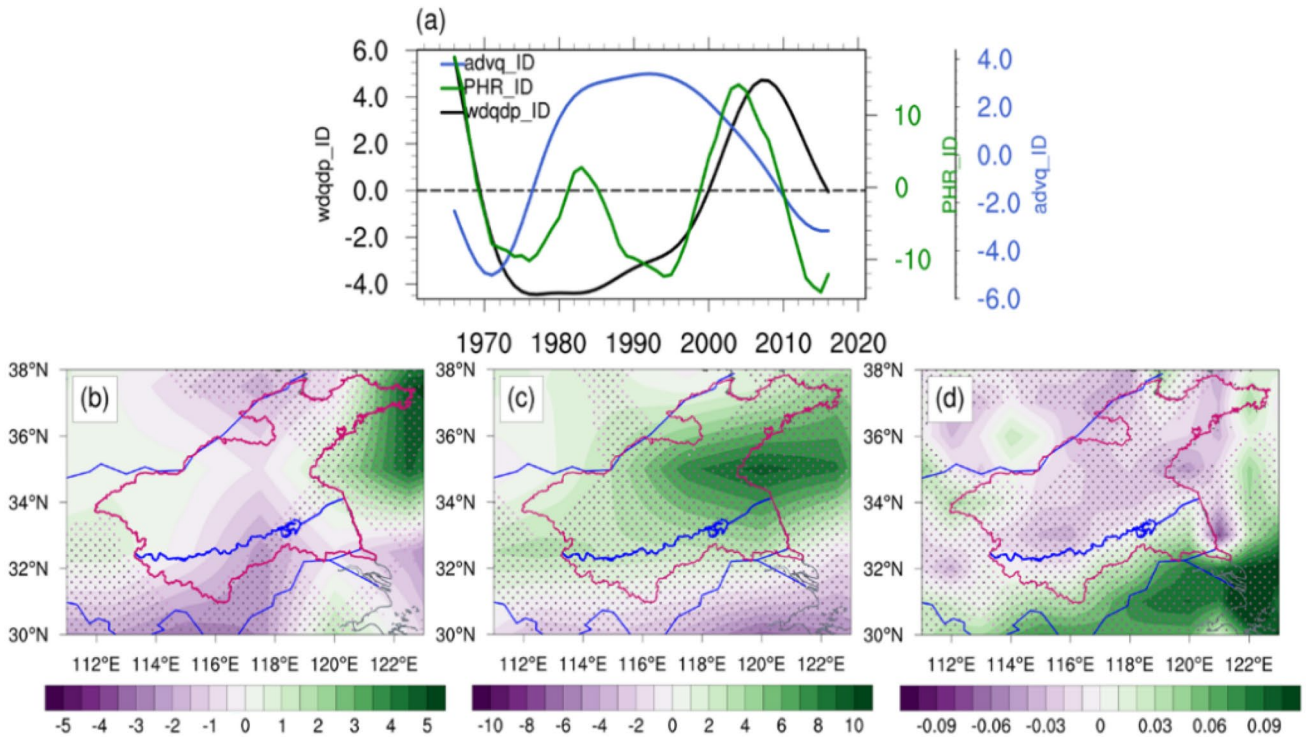

Fig. 6 **a** Time series of interdecadal variation of regional mean PHR (green solid line, unit: mm day^{-1}), water vapor advection term (blue solid line, unit: kg m^{-2} s^{-1}) and vertical water vapor transport term (black solid line, unit: kg m^{-2} s^{-1}) over the HRB in July–August of 1961–2021. Regressions of **b** water vapor advection term, **c** vertical water vapor transport term, and **d** evaporation term (unit: kg m^{-2} s^{-1}) against the PHR index (dots indicate significance at the 95% confidence level)

Table 3 Correlation coefficients between each term of the moisture budget equation and PHR over the HRB, and their contributions to PHR in July–August (unit: %)

	Vertical transport term	Advection term	Evaporation
Correlation coefficients	0.751**	−0.02	−0.55*
Contribution	83.68	16.32	Small quantitative neglect

Significance levels are indicated as 95% (*), and 99% (**)

circulation configuration of atmospheric upper-level dispersion and lower-level convergence (Fig. 7, Table 4). PHR over the HRB has significant positive correlation with 500-hPa temperature advection and the vertical velocity of the 300–850-hPa integral. The correlation coefficient between the regional mean temperature advection and the vertical velocity is 0.72, and it passes the significance test at the 95% confidence level, indicating that the two have significant positive correlation. Because the latent heat release of rainfall can influence the horizontal circulation in the troposphere with an overall characteristic of baroclinicity, and because the baroclinic response of the atmospheric circulation to the latent heat release of rainfall is minimal in the mid-troposphere, i.e., at 500-hPa, the causal relationship between circulation anomalies and rainfall anomalies can be distinguished to exclude interference by rainfall and its feedback effects with the atmosphere (Sampe and Xie 2010; Wang 2017). The above analysis also shows that the interdecadal variation in PHR over the HRB is governed by interdecadal variation in local vertical motion, and that thermal effects have substantial impact on vertical motion over the HRB. The regression of diabatic heating against the basin-averaged 500-hPa temperature advection time series (Fig. 7d) shows that they have significant positive correlation, centered over the HRB and covering the region with the highest interdecadal variance in PHR in July–August (Fig. 4b). Thus, when the warm advection anomaly in the mid-troposphere over the HRB is elevated, the diabatic heating anomaly over this region is also enhanced, accompanied by ascending motion that ultimately leads to interdecadal enhancement of PHR. Additionally, the development of warm advection in the middle and lower troposphere also favors lower-atmospheric depressurization and higher-atmospheric pressurization, i.e., it favors the formation of lower-tropospheric low pressure and the strengthening of the upper-tropospheric ridge. Low pressure also favors the development of convergence and ascending motion, while

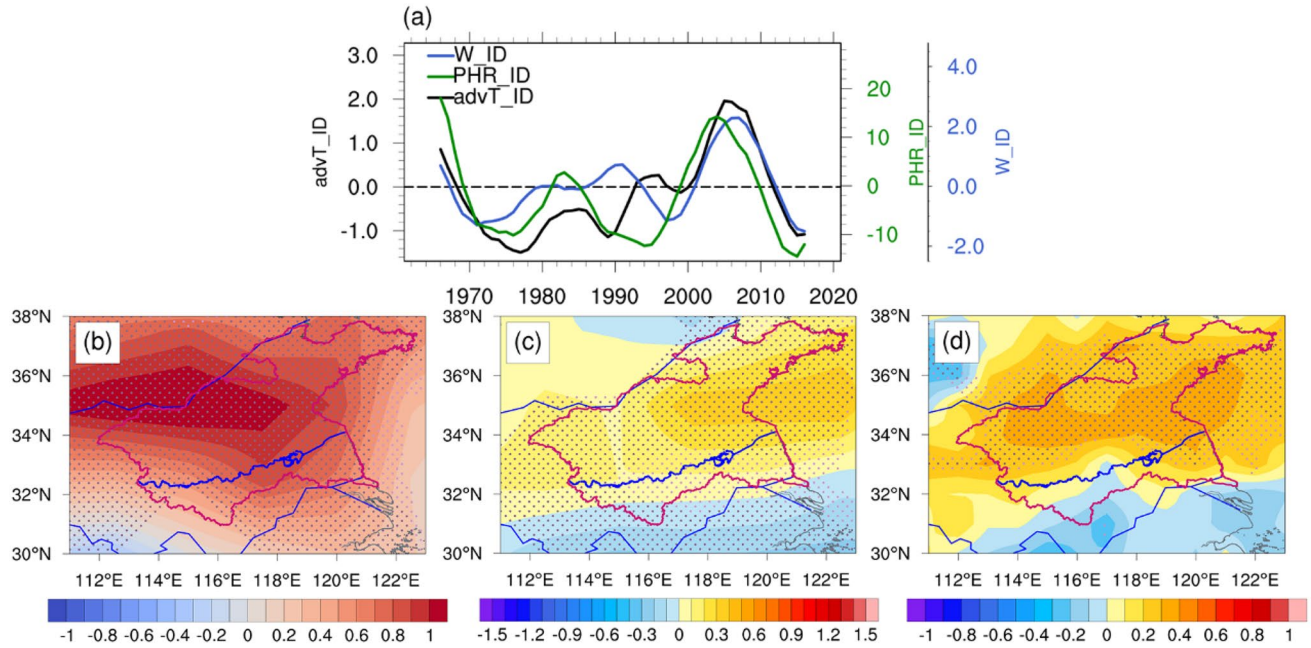

Fig. 7 **a** Time series of interdecadal component of regional mean PHR (green solid line, unit: mm day^{-1}), 500-hPa temperature advection (blue solid line, unit: K s^{-1}), and 300–850-hPa vertically integrated vertical velocity (black solid line, unit: m s^{-1}) over the HRB in July–August of 1961–2021. Regressions of **b** 500-hPa temperature advection (unit: K s^{-1}) and **c** 300–850-hPa vertically integrated vertical velocity (unit: m s^{-1}) against the PHR index, and **d** spatial distribution of the correlation coefficients between diabatic heating and temperature advection at 500-hPa (dots indicate significance at the 95% confidence level)

Table 4 Correlation coefficients between the PHR index and regional mean 300–850-hPa vertically integrated vertical velocity and 500-hPa temperature advection over the HRB

	Temperature advection	Vertical velocity
Correlation coefficients with PHR	0.720**	0.614**

Significance levels are indicated as 95% (*), and 99% (**)

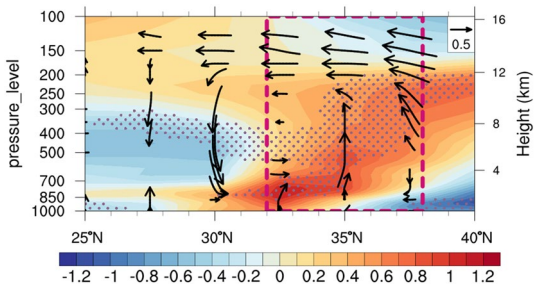

Fig. 8 Vertical profiles of regressions of regional mean (114°–120°E) pseudo-equivalent potential temperature (shading, unit: K) and wind (vector, unit: m s^{-1}) over the HRB against the PHR index in July–August of 1961–2021 (dots and bold vectors indicate significance at the 95% confidence level; dark pink dashed line indicates the location of the HRB)

the upper-tropospheric ridge favors the transport of cold air to the HRB and upper-tropospheric dispersion. The interdecadal correlation coefficient between basin-averaged 500-hPa temperature advection and the 200-hPa westerly jet index is − 0.61 (passing the significance test at the 95% confidence level), indicating that interdecadal enhancement of 500-hPa warm advection over the HRB might be caused primarily by interdecadal weakening of the westerly jet (interdecadal enhancement of the 200-hPa northerlies). Thus, atmospheric circulation anomalies can not only cause abnormal ascending motion over the HRB through dynamical impacts, but can also further boost ascending motion by changing the thermal distribution.

One of the major variables determining the static stability of the atmosphere is the pseudo-equivalent potential temperature, which can reflect the gravitational potential energy, internal energy, and latent heat energy of the atmosphere (Liao et al. 2022). From an energy perspective (Fig. 8), during the positive phase of PHR, the positive anomalous region of pseudo-equivalent potential temperature is over the HRB from 850 to 200-hPa, among which the entire region near 500-hPa is significantly positive. This indicates that 500-hPa warm advection might cause the atmosphere to become unstable, which is favorable for the development of anomalous convection. In contrast, the lower and middle troposphere to the south of the HRB (mostly over the YRB) has a negative anomaly of pseudo-equivalent potential

temperature, which leads to abnormal amplification of descending motion. Consequently, an anomalous meridional circulation forms over the HRB and the YRB, which is beneficial to the long-term stability of the anomalous system. The anomalously enhanced southerlies in the lower troposphere, which promote water vapor transport to the HRB in the lower troposphere, correspond to the anomalously enhanced northerlies in the upper troposphere, which combine with the anomalously enhanced ascending motion to create a circulation configuration favorable for rainfall. Furthermore, the distribution of positive pseudo-equivalent potential temperature anomalies over the HRB, and the distribution of negative pseudo-equivalent potential temperature anomalies over the YRB, lead to anomalous enhancement of the pseudo-equivalent potential temperature gradient over the region, which is the primary reason for the formation of the front in the middle and lower troposphere (Zheng et al. 2007; Liu et al. 2020; Huang et al. 2021). Consequently, the interdecadal increase in pseudo-equivalent potential temperature over the HRB also establishes an atmospheric background suitable for the generation of frontal rainfall.

3.3 Mechanisms of impact of AMO on PHR over the HRB

The importance of SST as external forcing of long-term climate change in East Asia has been well established (Zhou and Xia 2012; Si and Ding 2016; Si et al. 2021). Figure 9a displays the spatial distribution of the correlation coefficients between the PHR index and the interdecadal variation in global SST in July–August. The areas delineated by colored rectangles in Fig. 9a are designated as critical regions of SST because results demonstrate substantial correlation between the interdecadal variation in PHR over the HRB and the interdecadal variation in SST in the Atlantic, Pacific, and Indian oceans. There is also a region of moderately significant negative correlation in the South Atlantic, but it is ignored here owing to its small extent and its separation from the HRB. Here, the AMO and PO SST indexes are defined as the interdecadal variation in the regional mean SST anomalies in the North Atlantic and North Pacific critical regions, respectively. Because the North Pacific critical region coincides with the region for which the AMO index is calculated (Schlesinger and Navin 1994), the interdecadal variation of the SST index in the North Pacific critical region is in fact the AMO index. The Indian Ocean SST index (IO) is defined as the interdecadal variation in the leading mode time series of the empirical orthogonal function in the Indian Ocean critical region. The leading mode has the same pattern as the spatial distribution of correlation coefficients between the PHR index and SST in the Indian Ocean critical region. Among the three critical SST regions, AMO has the most significant effect on the interdecadal variation in PHR over the HRB in July–August (Table 5). On the one hand, AMO has significant positive correlation with PO, and when AMO is removed, the correlation coefficient between PHR in the HRB and the SST in the North Pacific changes from positive to negative, indicating that the interdecadal variation in AMO can modulate the interdecadal SST anomalies in the North Pacific. The influence of the Indian Ocean on PHR over the HRB is significantly weaker after excluding the influence of AMO, indicating that IO may also influenced by AMO. Furthermore, the strong correlation between AMO and PHR over the HRB persists almost from the previous autumn to peak in the summer of the same period, whereas the signals in the Pacific and Indian oceans appear sequentially in the spring and May of the same year (figure not shown), and even for the same period as AMO, the interdecadal transition is ahead of the PHR over the HRB.

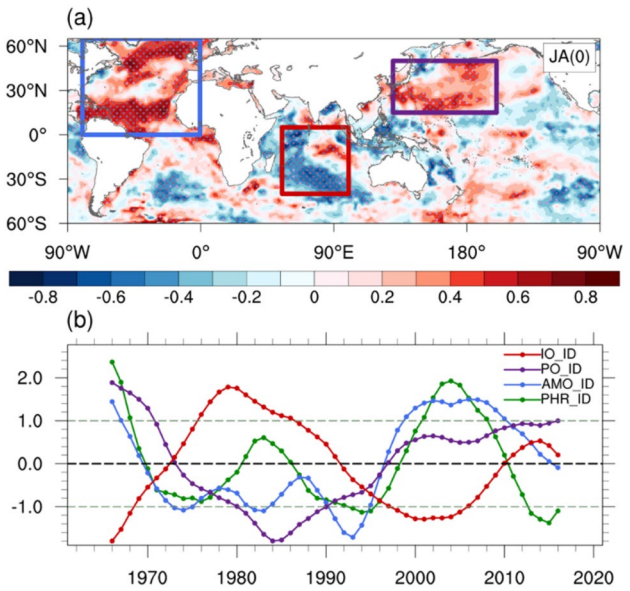

Fig. 9 **a** Spatial distribution of correlation coefficients between the PHR index and global SST in July–August 1961–2021 (dots indicate significance at the 95% confidence level; colored rectangles indicate critical SST regions), and **b** time series of interdecadal component of PHR (green line) and SST indexes in July–August 1961–2021 (blue, red, and purple lines indicate AMO, IO, and PO indexes, which correspond to the blue, red, and purple rectangles in **a**, respectively)

Table 5 Correlation coefficients and partial correlation coefficients between SST indexes and the PHR index, and correlation coefficients between AMO and PO/IO

	AMO	PO	IO
Correlation coefficients	0.708**	0.344	−0.515*
Partial correlation coefficients	0.942**	−0.364	−0.10
Correlation coefficients with AMO index	–	0.697**	−0.646**

Significance levels are indicated as 95% (*), and 99% (**)

The above analyses imply that in the late 1990s, AMO was the most important oceanic forcing. Therefore, the role of AMO in regulating PHR over the HRB during July–August is investigated further.

According to the partial regressions of interdecadal circulation and geopotential height in the upper–lower troposphere and vertical velocity in the mid-troposphere against AMO (Fig. 10), in the upper troposphere, the atmospheric circulation of a cyclone–anticyclone pair forms a wave train from the Atlantic Ocean to northeastern Asia that dominates the influence of AMO on the interdecadal variation in PHR over the HRB. This differs from the previously examined mechanism of influence of AMO in influencing the PDO to excite a lower tropospheric PJ pattern (Si and Ding 2016), suggesting that AMO does not have to influence rainfall over the HRB through the Pacific Ocean, which itself can modulate rainfall over the HRB. In the upper troposphere over the HRB, the AMO positive phase generates a wave train that induces a major anticyclonic circulation anomaly centered over the YRB and an anomalous cyclone over northeastern China. The northern HRB is influenced by winds from the southern edge of the anomalous cyclone, while the southern HRB is influenced by winds from the western edge of the anomalous anticyclone, and there is marked enhancement in ascending motion. At 850-hPa, anomalous northerlies over the northern HRB and anomalous southwesterlies over the southern HRB can be observed, i.e., in both the middle and the lower troposphere, the AMO positive phase can lead to convergence of cold and warm air currents over the HRB. Additionally, AMO can force an anomalous anticyclone–cyclone pair over the HRB and northeastern China by exciting a wave train, which transports warm humid air from lower latitudes and cold dry air from higher latitudes to the HRB, resulting in enhanced convection over the HRB. Moreover, while the cyclonic anomaly over northeastern China weakens from the upper troposphere downward, its position is displaced constantly southward, gradually moving to the northern HRB. Therefore, the circulation configuration of the upper-tropospheric anticyclone and lower-tropospheric cyclone can also lead to enhancement of ascending motion. In contrast, almost the entire troposphere over South China is controlled by an anomalous anticyclonic circulation, which causes descending motion and forms an anomalous meridional circulation over both the HRB and the YRB, consistent with the regression results against the PHR index. Additionally, the warm SST anomaly in the North Pacific, which in turn causes the formation of low-level PJ-like patterns, might be forced by the anomalous anticyclone over the region that is generated by AMO. There are some differences between the results of AMO partial regression and PHR regression. That is mainly because the formation of the anticyclone over Lake Baikal is little influenced by AMO. Zhu et al. (2023) indicated that tropospheric temperature anomalies over the Tibetan Plateau can lead to the anomalous anticyclone over Lake Baikal. Therefore, the synergistic effect of the ocean and Tibetan Plateau is worth further research.

The partial regression of PHR against AMO (Fig. 11a) also shows that the AMO positive phase can lead to

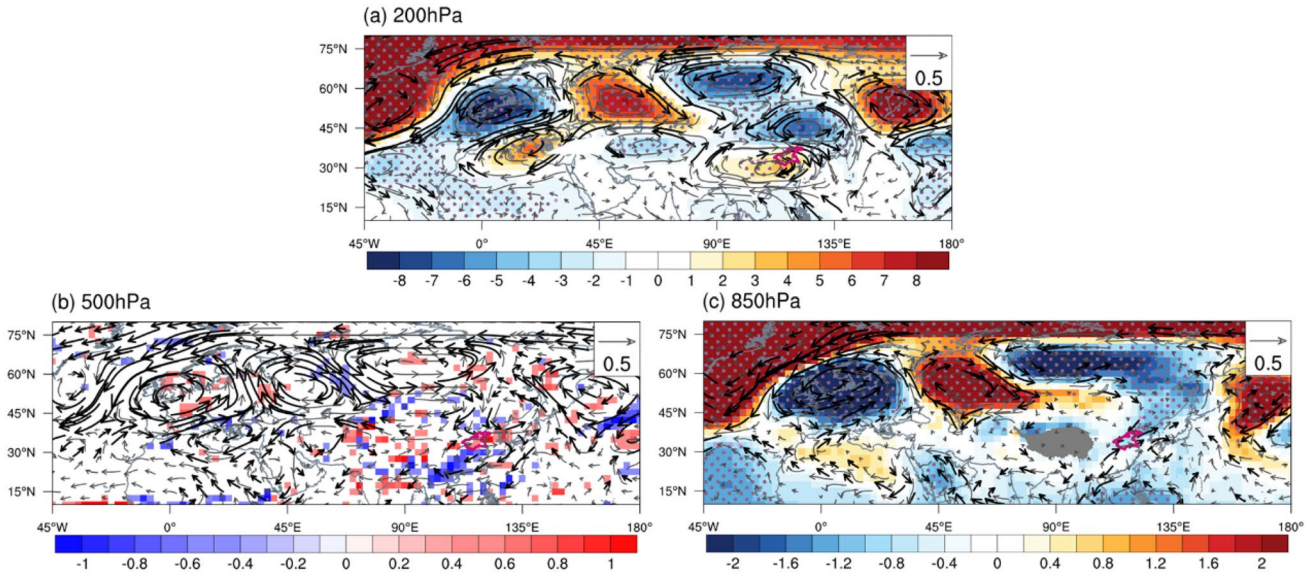

Fig. 10 Partial regressions of **a** 200-hPa and **c** 850-hPa geopotential height field (shading, unit: gpm) and wind (vector, unit: m s^{-1}), and **b** 500-hPa vertical velocity (shading, unit: m s^{-1}) and wind (vector, unit: m s^{-1}) against AMO in July–August of 1961–2021 [excluding the effects of the Indian Ocean (IO) and Pacific Ocean (PO) indexes; dots and bold vectors indicate significance at the 95% confidence level; only regions that passed the significance test are shown in **b**]

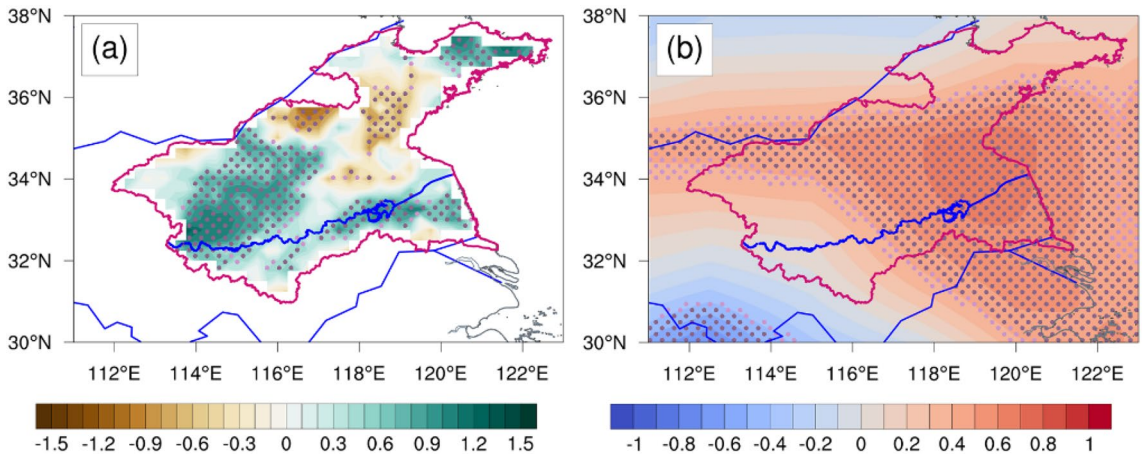

Fig. 11 Partial regressions of **a** PHR (unit: mm) and **b** 500-hPa temperature advection (unit: K s^{-1}) against AMO over the HRB in July–August of 1961–2021 (dots indicate significance at the 95% confidence level)

significant increase in PHR over most areas of the HRB, and that these areas correspond well to the areas with high interdecadal variance (Fig. 4b), indicating that AMO plays an important role in modulating the interdecadal variation in PHR over the HRB. The partial regression of 500-hPa temperature advection against AMO also exhibits significant positive anomalies over the HRB (Fig. 11b), although its center is further northeastward in comparison with that of the PHR center owing to the strong baroclinic characteristics of the mid-latitude atmosphere (Fang and Yang 2016). The AMO interdecadal phase transition plays a major role in modulating the interdecadal variation in thermal conditions over the HRB.

The AMO positive phase can cause anomalous enhancement of ascending motion, instability, a meridional secondary circulation between the HRB and the YRB, and southerlies in the lower atmosphere (Fig. 12a). The partial regression of wave activity flux profile against the AMO (Fig. 12b) indicates that the Rossby wave sources in the upper troposphere exhibit a "+−+−+" wave train, with positive anomalies centered over the North Atlantic, Central Asia, and northeastern Asia, and negative anomalies centered over Western Europe, Lake Baikal, and the HRB. Accordingly, a teleconnection wave train from the North Atlantic to the middle and high latitudes of East Asia can be excited by the AMO positive (negative) phase, resulting in a positive (negative) geopotential height anomaly in the upper troposphere over the HRB. The wave train originates from the North Atlantic at approximately 45°–20°W and moves through the middle–high latitudes of the Northern Hemisphere to the HRB. The locations of its centers are consistent with those of the geopotential height anomalies and the Rossby wave source anomalies (Fig. 12c). Furthermore, the anomalous propagation of energy caused by the interdecadal phase transition of AMO leads to enhancement of the upper-tropospheric northerlies over the HRB, which in turn facilitates enhancement of the middle- and lower-tropospheric southerlies, i.e., enhancement of warm advection and increase in PHR.

3.4 Impact of PDO phase transition on PHR over the HRB

As an important factor affecting the summer precipitation in East Asia, PDO's regulating effect on the East Asian summer monsoon and its precipitation has been extensively studied (Feng et al. 2014; Chinta et al. 2022). Therefore, next we made a brief discussion about the PDO effects on PHR over the HRB in July and August.

In the entire period (1961–2021), the correlation coefficient between PHR index and PDO is only − 0.203, which doesn't pass the significance test. However, the phase transition of PDO in the late 1990s can enhance both the WNPSA at 500-hPa (Fig. 13b) and the anomalous anticyclone over the Northwestern Pacific Ocean at 850-hPa (Fig. 13c), which contributes the water vapor transport to the HRB (Fig. 14). Because the relationship between PHR index and PDO changed after late 1980s (correlation coefficient changing from 0.337 to − 0.406) and the data loss caused by the interdecadal filtering, the composite analysis is performed only in the periods of 1989–1999 and 2000–2015. PDO may have little effect on the transport of cold air from high latitude due to the anomalous southwesterly over the north of the HRB (Fig. 13a).

3.5 Verification with numerical experiments

The hist-resAMO experiment can better replicate the interdecadal variation in AMO (Fig. 15), and the correlation coefficient between the simulated AMO index and the

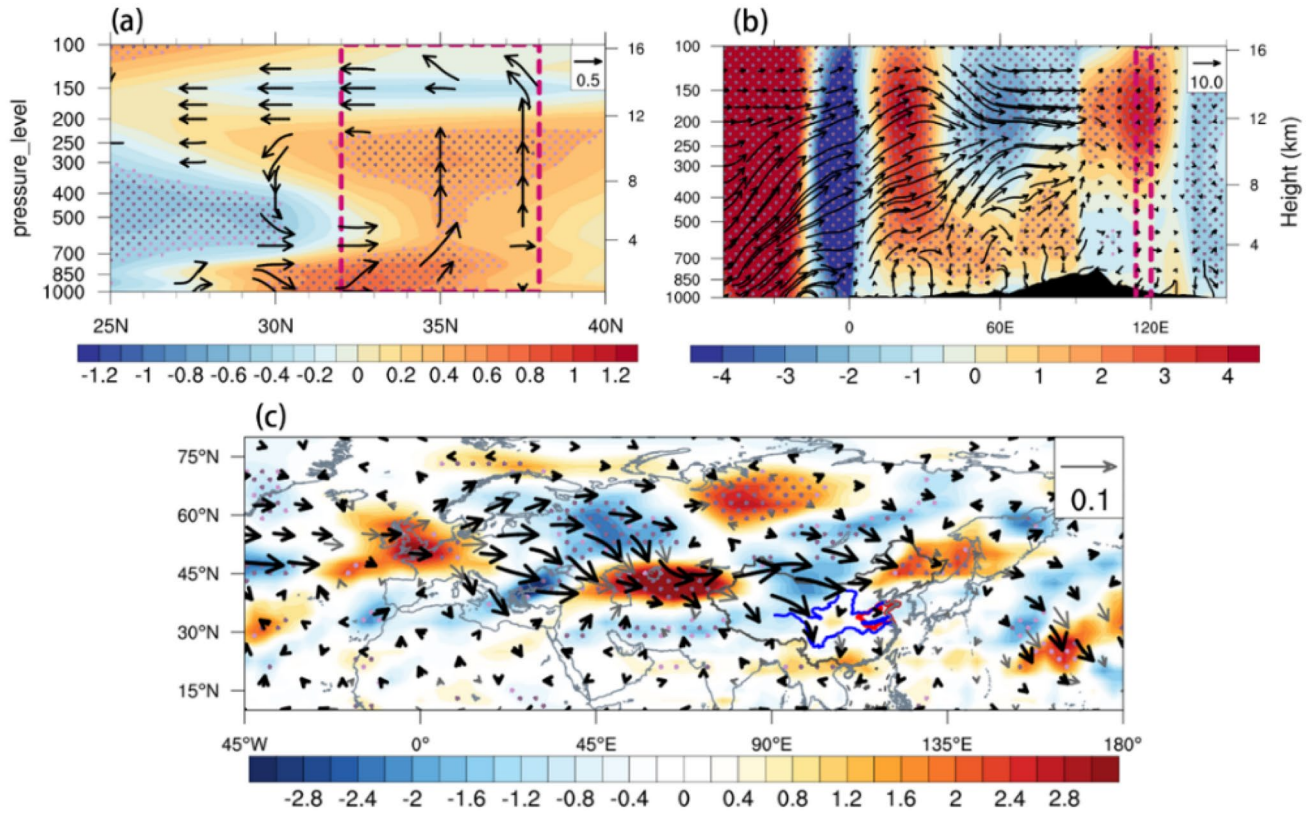

Fig. 12 **a** Vertical profiles of partial regressions of regional mean (114°–120°E) pseudo-equivalent potential temperature (shading, unit: K) and wind (vector, unit: m s^{-1}) over the HRB against AMO, **b** vertical profiles of partial regressions of wave activity flux (unit: m^2 s^{-2}) and geopotential height (unit: gpm) along an inclined path between (60°N, 45°W) and (30°N, 150°E) against AMO in July–August of 1961–2021, and **c** partial regressions of 200-hPa wave activity flux (vector, unit: m^2 s^{-2}) anomaly and Rossby wave source anomaly (shading, unit: 10^{-10} s^{-2}) against AMO (dots and bold vectors indicate significance at the 95% confidence level)

AMO index derived from HadISST is 0.94. In 1996/1997, AMO shows interdecadal transition from a negative phase in 1986–1996 to a positive phase in 1997–2007. However, there are differences between the simulated AMO's phase with the observation during 1975–1986, which might have implications for subsequent simulations with the hist-resAMO experiment; therefore, the following analysis is primarily performed using the simulation results for the 20 years before and after the 1990s (1986–2007). On the interdecadal time scale, the correlation coefficient between the simulated AMO and PHR is 0.889 and that between the observed AMO and PHR is 0.797 from 1986 to 2007. In the hist-resAMO experiment, interdecadal transition from a negative phase to a positive phase occurred in PHR over the HRB in 1998/1999 (Fig. 16a). It is evident that PHR over the HRB is substantially increased when AMO is in positive phase (Fig. 16b) and substantially diminished when AMO is in negative phase (Fig. 16c), which indicates that the interdecadal transition of PHR is modulated by the interdecadal phase shift of AMO. The reason for the difference between the simulated PHR and the AMO partial regression of PHR may be that although the model can basically simulate the key circulation systems, it also has some deviation in their position and intensity. In addition, the simulation ability of the model to extreme events is still limited.

Taking account of the AMO forcing, the upper troposphere exhibits a notable "+−+−+" wave train from the Atlantic Ocean to the HRB (Fig. 17a). Substantial anticyclonic (cyclonic) anomalies control the upper (lower) troposphere over the HRB. The model can also produce the anomalous cyclone over northeastern Asia and the anomalous enhancement of the WNPSH (Fig. 17b). Additionally, warm advection is substantially enhanced over the southern HRB, which can enhance the regional diabatic heating over the HRB, while cold advection is weakened over west north of the HRB (Fig. 18a). The model is also possible to replicate accurately the anomalous energy propagation in the upper troposphere (Fig. 18b). The above analysis demonstrates how effectively the hist-resAMO experiment can imitate the AMO signal, and further demonstrates how AMO modulates the interdecadal variation in PHR over the HRB.

In conclusion, the AMO interdecadal phase transition modulates the interdecadal variation in PHR over the HRB in two ways. On the one hand, it can affect the upper- and

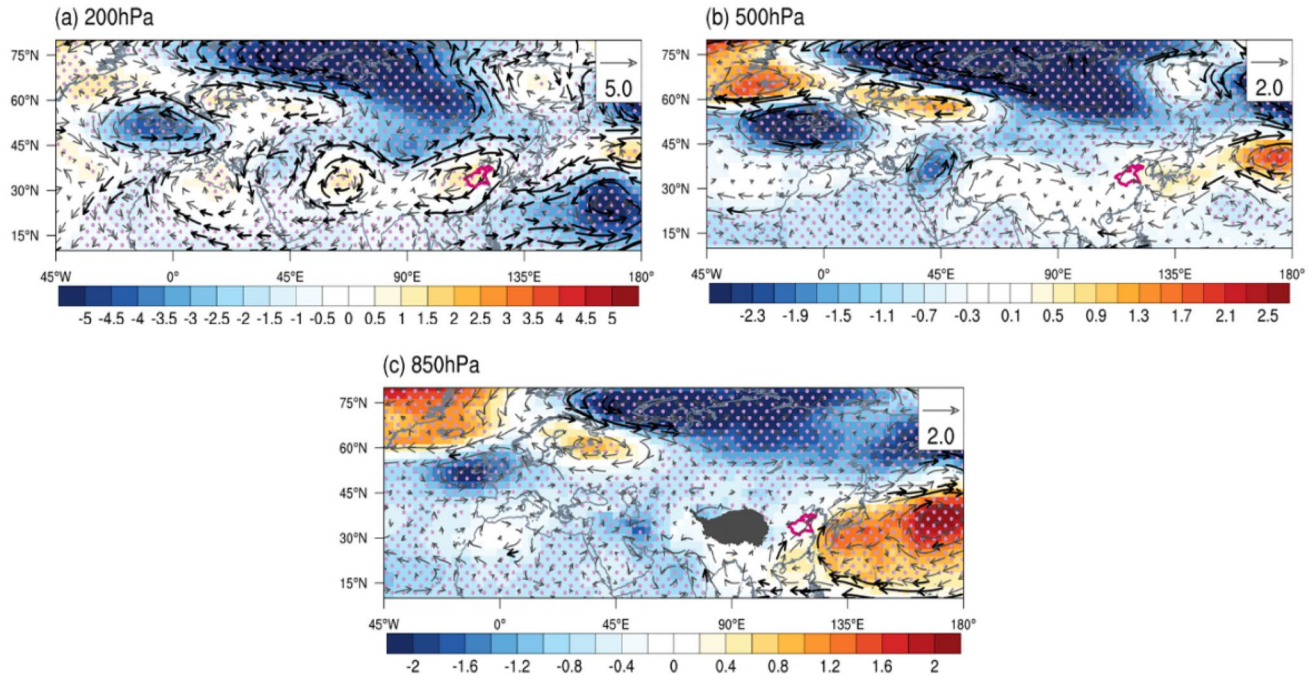

Fig. 13 Composite differences in **a** 200-hPa, **b** 500-hPa, and **c** 850-hPa geopotential height (shading, unit: gpm) and wind (vector, unit: m s^{-1}) between negative PDO phase (2000–2014) and positive PDO phase (1989–1999) (dots and bold vectors indicate significance at the 95% confidence level)

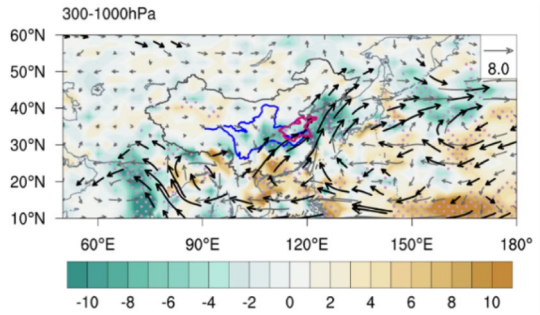

Fig. 14 Composite differences in 300–1000-hPa vertically integrated water vapor flux (vector, unit: kg $m^{-1}s^{-1}$) and its divergence (shading, unit: kg $m^{-1}s^{-1}$) between negative PDO phase (2000–2014) and positive PDO phase (1989–1999; dots and bold vectors indicate significance at the 95% confidence level)

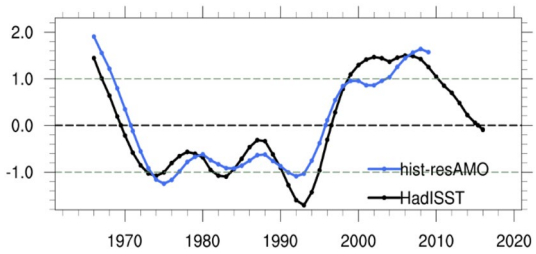

Fig. 15 Time series of interdecadal component of AMO in July–August (black line is derived from HadISST data, blue line is the outcome of the hist-resAMO experiment)

lower-tropospheric circulation configuration and mid-tropospheric temperature advection by energizing upper-tropospheric wave trains, thereby enhancing ascending motion over the HRB that causes interdecadal enhancement of PHR. On the other hand, AMO promotes water vapor transport to the HRB, in a manner described in earlier research (Si and Ding 2016), by influencing the wave train over the Pacific Ocean. The crucial mechanism in these two configurations is how AMO influences the interdecadal variation in vertical motion over the HRB.

4 Conclusions and discussion

Based on the above analysis of the distribution characteristics, interdecadal variation characteristics, and mechanisms of summer PHR over the HRB, and on examination of the modulating effect of AMO on the interdecadal transition in PHR in the late 1990s, the following conclusions can be drawn.

Summer PHR over the HRB occurs primarily in July and August with characteristics of significant interdecadal variation. A significant interdecadal phase transition from negative to positive occurred in 1998/1999, and the interannual variation is stronger when PHR is in positive

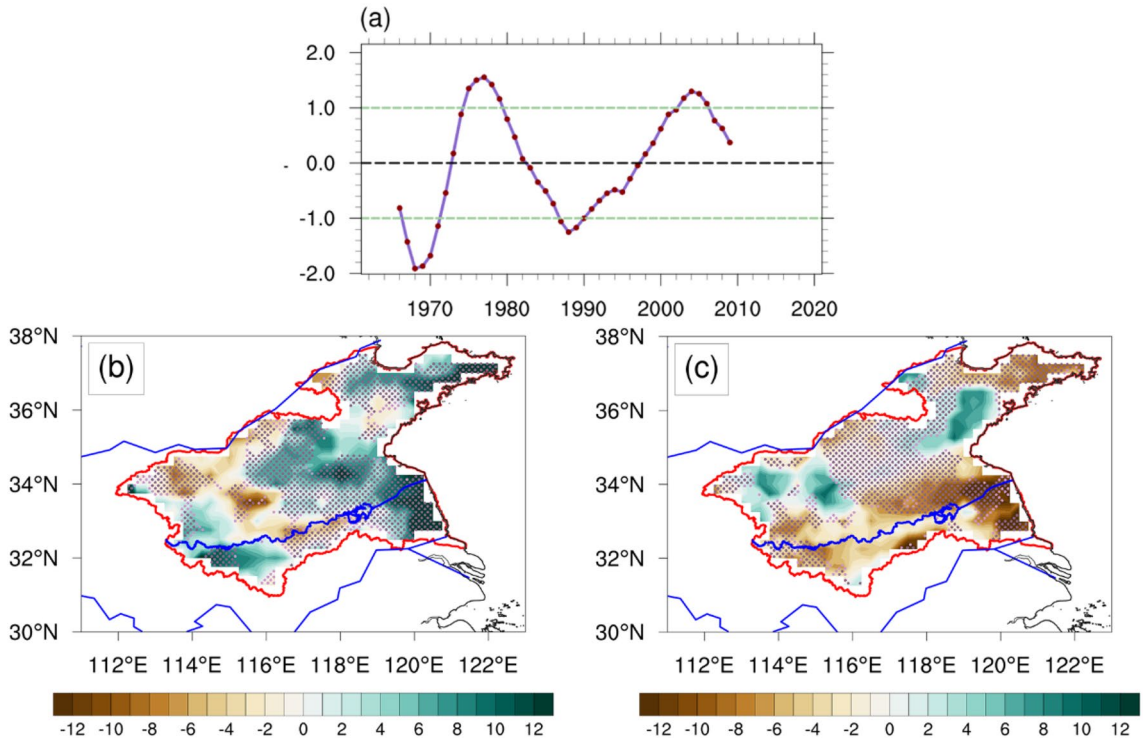

Fig. 16 **a** Time series of interdecadal component of PHR over the HRB derived from the hist-resAMO experiment for July–August of 1961–2014. Composite differences in PHR over the HRB between **b** positive AMO phase (1997–2007) and whole period (1986–2007), and **c** negative AMO phase (1986–1996) and whole period (1986–2007) in hist-resAMO experiment (unit: mm; dots indicate significance at the 95% confidence level)

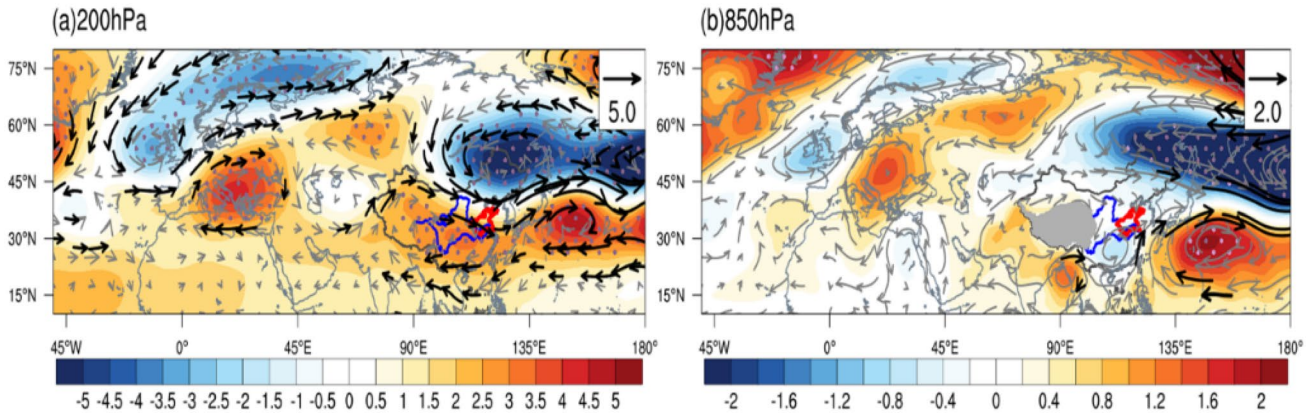

Fig. 17 Composite differences in **a** 200-hPa and **b** 850-hPa geopotential height (shading, unit: gpm) and wind (vector, unit: m s^{-1}) between positive AMO phase (1997–2007) and whole period (1986–2007) in hist-resAMO experiment (dots and bold vectors indicate significance at the 95% confidence level)

phase. The interdecadal enhancement in atmospheric ascending motion over the HRB is the dominant factor in the interdecadal increase in PHR. The most important external forcing responsible for the interdecadal transition is AMO. There are two aspects to the AMO modulation of interdecadal variation in PHR over the HRB. On the one hand, owing to the circulation configuration of upper-tropospheric divergence and lower-tropospheric convergence, the AMO positive phase excites a wave train in the upper troposphere at middle and high latitudes, resulting in an anomalous anticyclone and a weakened westerly jet in the upper troposphere over the HRB, and generates an anomalous cyclone and anomalously enhanced ascending motion in the lower troposphere

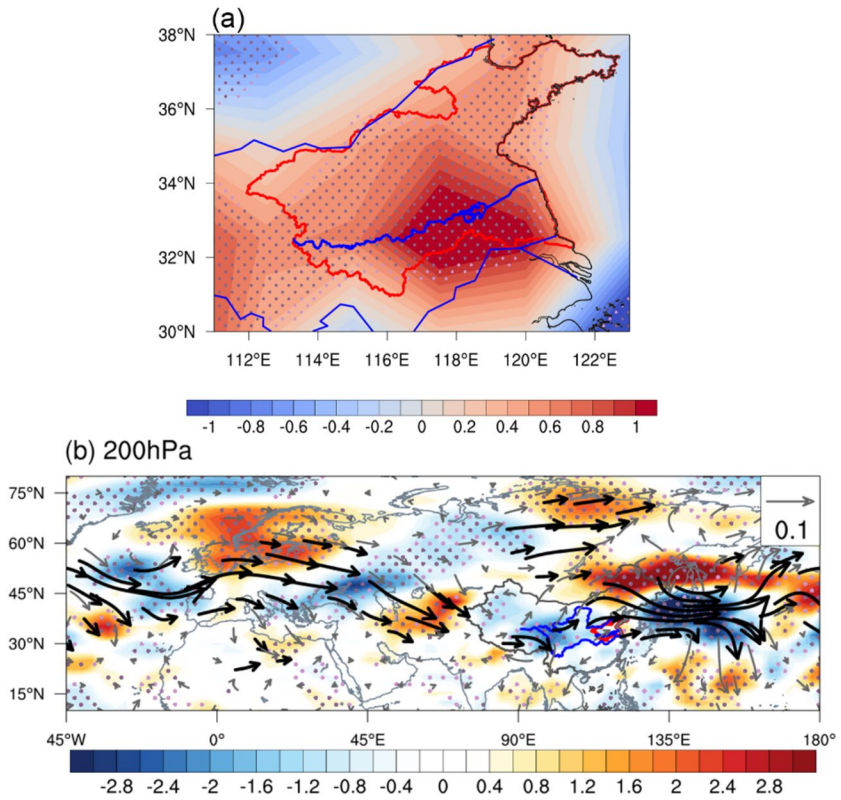

Fig. 18 Composite differences in **a** 500-hPa temperature advection anomaly (shading, unit: K s^{-1}) and **b** 200-hPa wave activity flux anomaly (vector, unit: m^2 s^{-2}) and Rossby wave source anomaly (shading, unit: 10^{-10} s^{-2}) between positive AMO phase (1997–2007) and whole period (1986–2007) in hist-resAMO experiment (dots and bold vectors indicate significance at the 95% confidence level)

over the HRB. Concurrently, an anomalous anticyclone governs almost the entire troposphere over the YRB, and an anomalous meridional circulation forms between the HRB and the YRB, with enhanced northerlies in the upper troposphere and enhanced southerlies in the middle and lower troposphere over the HRB. The anomalous southerlies provide anomalous warm advection and improved transport of warm-humid air from lower latitudes to the HRB. At the same time, AMO causes an anomalous cyclone over northeastern China that transports cold air from higher latitudes to the HRB, where the cold-dry air from the north meets the warm-humid air from the south, enhancing convection and favoring the occurrence and maintenance of PHR. On the other hand, by affecting sea surface temperature in the western North Pacific Ocean (Si and Ding 2016), the AMO can also indirectly trigger PJ-like wave train from the tropical Pacific Ocean to northeastern Asia, thus can result in the region of the Yellow Sea and the northwestern Pacific east of the HRB being under the control of an anomalous anticyclone. This enhances the transport of water vapor from the Pacific Ocean to the HRB, leading to increase in PHR over the HRB. The key mechanism among them is the impact of AMO on the interdecadal variation in vertical motion over the HRB.

In this study, we demonstrated the modulating effect of AMO on the interdecadal increase in PHR in July–August over the HRB in 1998/1999, and revealed that interdecadal enhancement in ascending motion is the determining factor. The influence of PDO on PHR over the HRB from July to August is also briefly discussed. However, because the relationship between PDO and East Asia summer precipitation is unstable (Gao 2006; Ding et al. 2018) and the data length is limited, the mechanisms of PDO's influence on PHR is still unclear. More research is needed to determine whether the transition of the relationship between PHR over the HRB and PDO is influenced independently by PDO or also by AMO's modulation. In addition, some studies also indicated that AMO and PDO may have joint-influence on the interdecadal variation of summer precipitation over the East Asia (Zhang et al. 2018). Therefore, it is necessary to further study the relationship between AMO and PDO as well as their joint-influence on PHR, which is of great significance to improve the interdecadal forecasting skills. However, only the external forcing of oceans was considered in the present study. As the "third pole" of the planet, the Tibetan Plateau has substantial impact on the climate of downstream regions. It has been demonstrated that snow cover over the Tibetan Plateau represents another external forcing that also has an important modulating effect on the interdecadal variation in summer rainfall over East Asia (Ding et al. 2013; Zhu et al. 2014; Lu et al. 2019), and that the atmospheric heat source over the Tibetan Plateau can play a role in the process via which AMO influences

summer rainfall over East Asia (Yu et al. 2023). AMO can also modulate the effect of the Tibetan Plateau on climate (Lu et al. 2019); however, connecting the influence of the oceans and of the plateau to summer rainfall over the HRB has not been well studied. Further research is also required on other issues such as the acceleration of the global water cycle due to global warming (Liu et al. 2021a, b) and how human activities might affect PHR over the HRB.

Author contributions All authors contributed to the study conception and design. Material preparation, data collection and analysis were performed by JY, QL and ZW. The first draft of the manuscript was written by JY and all authors commented on previous versions of the manuscript. All authors read and approved the final manuscript.

Funding This work was supported by the National Key Research and Development Program of China (2022YFE0136000), National Natural Science Foundation of China (U2242207), Second Tibetan Plateau Scientific Expedition and Research Program of China (2019QZKK0208), Natural Science Foundation of Anhui Province of China (2208085UQ08), National Natural Science Foundation of China (42105037).

Data availability The ERA5, HadISST and CN05.1 datasets used in this study are available in https://cds.climate.copernicus.eu, https://climatedataguide.ucar.edu and https://ccrc.iap.ac.cn/resource/detail?id=228, respectively.

Declarations

Conflict of interest The authors have no competing interests to declare that are relevant to the content of this article.

References

Bao M (2007) The statistical analysis of the persistent heavy rain in the last 50 years over China and their backgrounds on the large scale circulation. Chin J Atmosp Sci 31:779–792. https://doi.org/10.3878/j.issn.1006-9895.2007.05.03. (**in Chinese**)

Chen Y, Zhai PM (2013) Persistent extreme precipitation events in China during 1951–2010. Clim Res 57:143–155. https://doi.org/10.3354/cr01171

Chen D, Chen JL, Huang RH, Liu Y (2016) Interdecadal changes of summertime heavy rainfall in eastern China and their large-scale circulation backgrounds. Chin J Atmosp Sci 40:581–590. https://doi.org/10.3878/j.issn.1006-9895.1504.15144. (**in Chinese**)

Chinta V, Chen ZS, Du Y, Chowdary JS (2022) Influence of the Interdecadal Pacific oscillation on South Asian and East Asian summer monsoon rainfall in CMIP6 models. Clim Dyn. https://doi.org/10.1007/s00382-021-05992-6

Chou C, Lan C-W (2012) Changes in the annual range of precipitation under global warming. J Clim 25:222–235. https://doi.org/10.1175/JCLI-D-11-00097.1

Ding YH, Sun Y (2001) A study on anomalous activities of east Asian summer monsoon during 1999. J Meteorol Soc Jpn Ser II 79:1119–1137. https://doi.org/10.2151/jmsj.79.1119

Ding YH, Sun Y, Wang ZY, Zhu YX, Song YF (2009) Inter-decadal variation of the summer precipitation in China and its association with decreasing part II: possible causes. Int J Climatol 29:1926–1944. https://doi.org/10.1002/joc.1759

Ding YH, Sun Y, Liu YY et al (2013) Interdecadal and interannual variability of the Asian summer monsoon and its projection of future change. Chin J Atmosp Sci 37:253–280. https://doi.org/10.3878/j.issn.1006-9895.2012.12302. (**in Chinese**)

Ding YH, Si D, Liu YJ, Wang ZY, Liu Y, Zhao L, Song YF (2018) On the characteristics, driving forces and inter-decadal variability of the East Asian summer Monsoon. Chin J Atmos Sci 42:533–558. https://doi.org/10.3878/j.issn.1006-9895.1712.17261. (**in Chinese**)

Ding YH, Hu W, Huang Y, Chen FJ (2020a) The main scientific achievements of the first China-Japan cooperative GAME/HUBEX experiments: a historical review. Acta Meteorol Sin 78:721–734. https://doi.org/10.11676/qxxb2020.064. (**in Chinese**)

Ding YH, Liang P, Liu YJ, Zhang YC (2020b) Multiscale variability of Meiyu and its prediction: a new review. J Geophys Res-Atmos. https://doi.org/10.1029/2019JD031496

Ding YH, Liu YY, Hu Z-Z (2021) The record-breaking Meiyu in 2020 and associated atmospheric circulation and tropical SST anomalies. Adv Atmos Sci 38:1980–1993. https://doi.org/10.1007/s00376-021-0361-2

Enfield DB, Mestas-Nuñez AM, Trimble PJ (2001) The Atlantic multidecadal oscillation and its relation to rainfall and river flows in the continental U.S. Geophy Res Lett 28:2077–2080. https://doi.org/10.1029/2000GL012745

Fang JB, Yang X-Q (2016) Structure and dynamics of decadal anomalies in the wintertime midlatitude North Pacifc ocean-atmosphere system. Clim Dynam 47:1989–2007. https://doi.org/10.1007/s00382-015-2946-x

Feng J, Wang L, Chen W (2014) How does the east Asian summer monsoon behave in the decaying phase of El Nino during different PDO phases? J Clim 27:2682–2698. https://doi.org/10.1175/JCLI-D-13-00015.1

Gao H (2006) Decadal variation of the relationship between summer precipitation along the Huaihe River Valley and SST over the equatorial eastern Pacific (**in Chinese**). J Appl Meteorol Sci 17:1–9

Ha Y, Zhong Z, Chen HS, Hu YJ (2016) Out-of-phase decadal changes in boreal summer rainfall between Yellow-Huaihe river valley and Southern China around 2002/2003. Clim Dyn 47:137–158. https://doi.org/10.1007/s00382-0152828-2

Hersbach H, Bell B, Berrisford P et al (2020) The ERA5 global reanalysis. Q J Roy Meteor Soc 146:1999–2049. https://doi.org/10.1002/qj.3803

Huang RH, Chen JL, Liu Y (2011) Interdecadal variation of the leading modes of summertime precipitation anomalies over eastern China and its association with water vapor transport over East Asia (in Chinese). Chin J Atmosp Sci 35:589–606. https://doi.org/10.3878/j.issn.1006-9895.2011.04.01

Huang ZY, Wang JY, Zhou W (2021) Characteristics analysis of an extreme heavy rain event in the middle reaches of the Yangtze River from July 4 to 8 in 2020. Torrential Rain Disaster

40:333–341. https://doi.org/10.3969/j.issn.1004-9045.2021.04.001. (**in Chinese**)

Jin HY, Chen XH, Zhong RD et al (2022) Spatiotemporal distribution analysis of extreme precipitation in the Huaihe River basin based on continuity. Nat Hazards 114:1–30. https://doi.org/10.1007/s11069-022-05534-1

Kosaka Y, Xie SP, Nakamura H (2011) Dynamics of interannual variability in summer precipitation over East Asia. J Clim 24:5435–5453. https://doi.org/10.1175/2011JCLI4099.1

Li XZ, Wen ZP, Zhou W, Wang DX (2012) Atmospheric water vapor transport associated with two decadal rainfall shits over East China. J Meteorol Soc Jpn Ser II 90:587–602

Li JP, Sun C, Jin FF (2013) NAO implicated as a predictor of Northern Hemisphere mean temperature multidecadal variability. Geophy Res Lett 40:5497–5502. https://doi.org/10.1002/2013GL057877

Liang X-Z, Wang W-C (1998) Associations between China monsoon rainfall and tropospheric jets. Q J Roy Meteor Soc 124:2597–2623. https://doi.org/10.1002/qj.49712455204

Liao RW, Liu G, Chen JM, Zhang L (2022) Interdecadal variability of summer extreme rainfall events over the Huaihe River Basin and associated atmospheric circulation. Atmosphere 13:1189. https://doi.org/10.3390/atmos13081189

Lin PF, Yu ZP, Lü JH, Ding MR, Hu AX, Liu HL (2019) Two regimes of Atlantic multidecadal oscillation: cross-basin dependent or atlantic-intrinsic. Sci Bull 64:198–204. https://doi.org/10.1016/j.scib.2018.12.027

Liu BQ, Yan YH, Zhu CW, Ma SM, Li JY (2020) Record-breaking Meiyu rainfall around the Yangtze River in 2020 regulated by the subseasonal phase transition of the North Atlantic Oscillation. Geophys Res Lett. https://doi.org/10.1029/2020GL090342

Liu YB, Zhang C, Tang QH et al (2021a) Moisture source variations for summer rainfall in different intensity classes over Huaihe River Valley, China. Clim Dyn 57:1121–1133. https://doi.org/10.1007/s00382-021-05762-4

Liu MF, Gabriel AV, Brian S, Yang WC (2021b) Enhanced hydrological cycle increases ocean heat uptake and moderates transient climate sensitivity. Nat Clim Change 11:848–853. https://doi.org/10.1038/s41558-021-01152-0

Lu RY (2004) Associations among the components of the East Asian summer monsoon system in the meridional direction. J Meteorol Soc Japan Ser II 82:155–165. https://doi.org/10.2151/jmsj.82.155

Lu MM, Huang BH, Li ZN, Yang S (2019) Role of Atlantic air–sea interaction in modulating the effect of Tibetan Plateau heating on the upstream climate over Afro-Eurasia–Atlantic regions. Clim Dyn 53:509–519. https://doi.org/10.1007/s00382-018-4595-3

Lu W, Zhu YM, Ha Y, Zhong Z, Hu YJ (2022) Recent decadal weakening of the summertime rainfall interannual variability over Yellow-Huaihe River Valley attributable to the western Pacific cooling. Front Earth Sci. https://doi.org/10.3389/feart.2022.946252

Ma ZG (2007) The interdecadal trend and shift of dry/wet over the central part of North China and their relationship to the Pacific Decadal Oscillation (PDO). Chin Sci Bull 52:2130–2139. https://doi.org/10.1007/s11434-007-0284-z

Piao JL, Chen W, Chen SF (2021) Water vapor transport changes associated with the interdecadal decrease in the summer rainfall over Northeast Asia around the late-1990s. Int J Climatol 41:E1469–E1482. https://doi.org/10.1002/joc.6780

Ping F, Tang XB, Gao ST, Luo ZX (2014) A comparative study of the atmospheric circulations associated with rainy-season floods between the Yangtze and Huaihe River basins. Sci China 57:1464–1479. https://doi.org/10.1007/s11430-013-4802-3

Pyper BJ, Peterman RM (1998) Comparison of methods to account for autocorrelation in correlation analyses of fish data. Can J Fish Aquat Sci 55:2127–2140. https://doi.org/10.1139/f98-104

Qian MK, Wang K (2017) Flood management in China: the Huaihe River basin as a case study. J Flood Risk Manag. https://doi.org/10.5772/intechopen.69047

Qiu S, Zhou W (2019) Variation in summer rainfall over the Yangtze River region during warming and hiatus periods. Atmosphere 10:173. https://doi.org/10.3390/atmos10040173

Ren XJ, Yang X-Q, Sun XG (2013) Zonal oscillation of western Pacific subtropical high and subseasonal SST variations during Yangtze persistent heavy rainfall events. J Clim 26:8929–8946. https://doi.org/10.1175/JCLI-D-12-00861.1

Sampe T, Xie SP (2010) Large-scale dynamics of the meiyu-baiu rainband: environmental forcing by the westerly jet. J Clim 23:113–134. https://doi.org/10.1175/2009JCLI3128.1

Schlesinger M, Navin R (1994) An oscillation in the global climate system of period 65–70 years. Nature 367:723–726. https://doi.org/10.1038/367723a0

Si D, Ding YH (2013) Decadal change in the correlation pattern between the Tibetan Plateau winter snow and the East Asian summer precipitation during 1979–2011. J Clim 26:7622–7634. https://doi.org/10.1175/JCLI-D-12-00587.1

Si D, Ding YH (2016) Oceanic forcings of the interdecadal variability in east Asian summer rainfall. J Clima 29:7633–7649. https://doi.org/10.1175/JCLI-D-15-0792.1

Si D, Jiang DB, Hu AX, Lang XM (2020) Variations in Northeast Asian summer precipitation driven by the Atlantic multidecadal oscillation. Int J Climatol. https://doi.org/10.1002/joc.6912

Si D, Jiang DB, Ding YH (2021) Synergistic impacts of the Atlantic and Pacific oceans on interdecadal variations of summer rainfall in Northeast Asia. J Meteorol Res 35:844–856. https://doi.org/10.1007/s13351-021-0191-2

Sun C, Li JP, Jin FF (2015) A delayed oscillator model for the quasi-periodic multidecadal variability of the NAO. Clim Dyn 45:2083–2099. https://doi.org/10.1007/s00382-014-2459-z

Sun C, Li JP, Ding RQ, Jin Z (2017a) Cold season Africa–Asia multidecadal teleconnection pattern and its relation to the Atlantic multidecadal variability. Clim Dyn 48:3903–3918. https://doi.org/10.1007/s00382-016-3309-y

Sun C, Kucharski F, Li JP, Jin FF, Kang IS, Ding RQ (2017b) Western tropical Pacific multidecadal variability forced by the Atlantic multidecadal oscillation. Nat Commun 8:1599. https://doi.org/10.1038/ncomms15998

Sun C, Li JP, Kucharski F, Xue JQ, Li X (2019) Contrasting spatial structures of Atlantic multidecadal oscillation between observations and slab ocean model simulations. Clim Dyn 52:1395–1411. https://doi.org/10.1007/s00382-018-4201-8

Tong X, Yan ZW, Zhou W, Xia JJ, Quan XW (2023) Multidecadal oceanic modulation of summer precipitation in North China in 1200-year global climate simulations. J Clim 36:6125–6138. https://doi.org/10.1175/JCLI-D-22-0693.1

Wang HJ (2001) The weakening of the Asian monsoon circulation after the end of 1970s. Adv Atmos Sci 18:376–386. https://doi.org/10.1007/BF02919316

Wang SX (2017) Effect of the Variation of East Asian westerly on the rainfall changes in Yangtze-Huaihe River Valley and North China (in Chinese). Dissertation, Lanzhou University

Wang T, Wang HJ, Odd HO, Gao YQ, Suo LL, Tore F, Yu L (2013) Anthropogenic agent implicated as a prime driver of shift in precipitation in eastern China in the late 1970s. Atmos Chem Phys 13:11997–12032. https://doi.org/10.5194/acp-13-12433-2013

Wei FY, Zhang T (2010) Oscillation characteristics of summer precipitation in the Huaihe River valley and relevant climate background. Sci China Earth Sci 53:301–316. https://doi.org/10.1007/s11430-009-0151-7

Wu J, Gao XJ (2013) A gridded daily observation dataset over China region and comparison with the other datasets (**in Chinese**). Chin J Geophys 56:1102–1111. https://doi.org/10.6038/cjg20130406

Xuan SL, Zhang QY, Sun SQ (2011) Anomalous midsummer rainfall in Yangtze River-Huaihe River valleys and its association with the East Asia westerly jet. Adv Atmos Sci 28:387–397. https://doi.org/10.1007/s00376-010-0111-3

Yao R, Ren XJ (2019) Decadal and interannual variability of persistent heavy rainfall events over the middle and lower reaches of the Yangtze River valley. J Meteorol Res 33:1031–1043. https://doi.org/10.1007/s13351-019-9070-5

Yin XX, Zhou LT, Huangfu JL (2021) Weakened connection between East China summer rainfall and the East Asia-Pacific teleconnection pattern. Atmosphere 12:704. https://doi.org/10.3390/atmos12060704

Yu LW, Si D, Jiang DB, Ding YH, Shen XY, Lang XM, Li QQ, Tian ZP (2023) Tibetan Plateau booster effect on the influence of Atlantic multidecadal variability on the East Asian summer rainfall. J Clim. https://doi.org/10.1175/JCLI-D-22-0472.1

Yuan Y, Yan DH, Yuan Z, Yin J, Zhao ZN (2019) Spatial distribution of precipitation in Huang-Huai-Hai River basin between 1961 to 2016. Int J Env Res Pub He 16:3404. https://doi.org/10.3390/ijerph16183404

Zhang QY, Guo H (2014) Circulation differences in anomalous rainfall over the Yangtze River and Huaihe River valleys in summer (**in Chinese**). Chin J Atmosp Sci 38:656–669. https://doi.org/10.3878/j.issn.1006-9895.1402.13240

Zhang ZQ, Sun XG, Yang X-Q (2018) Understanding the interdecadal variability of east Asian summer monsoon precipitation: joint influence of three oceanic signals. J Clim. https://doi.org/10.1175/JCLI-D-17-0657.1

Zhang J, Dong M, Wu TW et al (2019) BCC BCC-CSM2MR model output prepared for CMIP6 GMMIP hist-resAMO. Earth Syst Grid Federation. https://doi.org/10.22033/ESGF/CMIP6.2933. (**Accessed 3 June 2019**)

Zheng YG, Chen J, Ge GQ, Zhu PJ (2007) Typical structure, diversity and muti-scale characteristics of Meiyu front (**in Chinese**). Acta Meteorol Sin 65:760–772. https://doi.org/10.11676/qxxb2007.072

Zheng LN, Zhang ZH, Wang X, Jia XQ (2019) Relationship between East Asian summer monsoon anomaly and summer precipitation in Huanghuai region (**in Chinese**). Meteor Sci Technol 47:62–69. https://doi.org/10.19517/j.1671-6345.20180131

Zhou LT, Huang RH (2009) Interdecadal variability of summer rainfall in Northwest China and its possible causes. Int J Climatol 30:549–557. https://doi.org/10.1002/joc.1923

Zhou BT, Xia DD (2012) Interdecadal change of the connection between winter North Pacific oscillation and summer precipitation in the Huaihe River valley. Sci China Earth Sci 55:2049–2057. https://doi.org/10.1007/s11430-012-4499-8

Zhou TJ, Chen XL, He B, Wu B, Zhang LX (2019) Short commentary on CMIP6 global monsoons Model Intercomparison Project (GMMIP). Clim Change Res 15:493–497. https://doi.org/10.12006/j.issn.1673-1719.2019.132

Zhu YL, Wang HJ, Zhou W, Ma JH (2011) Recent changes in the summer precipitation pattern in East China and the background circulation. Clim Dyn 36:1463–1473. https://doi.org/10.1007/s00382-010-0852-9

Zhu YX, Liu HW, Ding YH, Zhang FY, Li W (2014) Interdecadal variation of spring snow depth over the Tibetan Plateau and its influence on summer rainfall over East China in the recent 30 years. Int J Climatol. https://doi.org/10.1002/joc.4239

Zhu YL, Wang HJ, Ma JH, Wang T, Sun JQ (2015) Contribution of the phase transition of Pacific decadal oscillation to the late 1990s' shift in East China summer rainfall. J Geophys Res-Atmos 120:8817–8827. https://doi.org/10.1002/2015JD023545

Zhu XY, Yang MZ, Liu G, Liu YJ, Li WJ, Nan SL, Sun LH (2023) A precursory signal of June–July precipitation over the Yangtze River Basin: December–January tropospheric temperature over the Tibetan Plateau. Adv Atmos Sci 40:1986–1997. https://doi.org/10.1007/s00376-022-2079-1